

Manuscript Number: MEP-D-17-00459R1

Title: Biomechanical Analysis of Bone Remodeling Following Mandibular Reconstruction using Fibula Free Flap

Article Type: Paper

Section/Category: Regular Issue Paper

Keywords: Fibula free flap; Finite element analysis; Jaw biomechanics; Mandibular reconstruction; Bone remodeling.

Corresponding Author: Dr. Nobuhiro Yoda,

Corresponding Author's Institution: Tohoku University Graduate School of Dentistry

First Author: Nobuhiro Yoda

Order of Authors: Nobuhiro Yoda; Keke Zheng; Junning Chen; Zhipeng Liao; Shigeto Koyama; Christopher Peck; Michael Swain; Keiichi Sasaki; Qing Li

Abstract: Whilst the newly established biomechanical conditions following mandibular reconstruction using fibula free flap can be a critical determinant for achieving favorable bone union, little has been known about their association in a time-dependent fashion. This study evaluated the bone healing/remodeling activity in reconstructed mandible and its influence on jaw biomechanics using CT data, and further quantified their correlation with mechanobiological responses through an in-silico approach. A 66-year-old male patient received mandibular reconstruction was studied. Post-operative CT scans were taken at 0, 4, 16 and 28 months. Longitudinal change of bone morphologies and mineral densities were measured at three bone union interfaces (two between the fibula and mandibular bones and one between the osteotomized fibulas) to investigate bone healing/remodeling events. Three-dimensional finite element models were created to quantify mechanobiological responses in the bone at these different time points. Bone mineral density increased rapidly along the bone interfaces over the first four months. Cortical bridging formed at the osteotomized interface earlier than the other two interfaces with larger shape discrepancy between fibula and mandibular bones. Bone morphology significantly affected mechanobiological responses in the osteotomized region ( $R^2 > 0.77$ ). The anatomic position and shape discrepancy at bone union affected the bone healing/remodeling process.



東北大学大学院歯学研究科  
Tohoku University Graduate School of Dentistry  
4-1 Seiryō-machi, Aoba-ku, Sendai 980-8575 Japan

**Dr. Nobuhiro Yoda**  
*Assistant Professor*

Division of Advanced Prosthetic Dentistry, Tohoku University Graduate School of Tohoku University Graduate School of Dentistry  
4-1 Seiryō-machi, Aoba-ku, Sendai 980-8575, JAPAN  
Telephone: +81-22-717-8369  
Facsimile: +81-22-717-8371  
Email: nobuhiro.yoda.e2@tohoku.ac.jp

24 February 2018

Dr Richard A Black, Editor-in-Chief  
*Medical Engineering & Physics*

Dear Dr Black,

First of all, we would like to take this chance to thank you for your kind consideration and editorial review of our paper. The editors and the reviewers indeed provided us with highly constructive comments and suggestions, which I believe helped us to make our paper in a much better quality.

Please find the revision of the manuscript and detailed point-by-point responses. We have carefully considered all the comments raised and seriously revised the paper. After many discussion sessions now we all agree to submit you our revision for your further consideration.

Thank you very much again for your consideration of the paper. We look forward to hearing from you at your earliest convenience.

Yours sincerely,

A handwritten signature in black ink that reads 'Nobuhiro Yoda'.

Nobuhiro Yoda, DDS, PhD

## Declaration

The authors affirm that this manuscript, entitled “Biomechanical Analysis of Bone Remodeling Following Mandibular Reconstruction using Fibula Free Flap” has been submitted solely to *Medical Engineering & Physics* and that it is not concurrently under consideration for publication in another journal.

The authors also confirm that the submitted work, including images, are original and there is no conflict of interest in this submitted work.

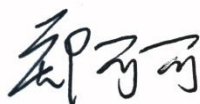
### Authors

### Signatures

Nobuhiro Yoda



Keke Zheng



Junning Chen



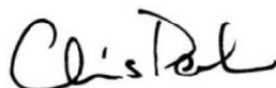
Zhipeng Liao



Shigeto Koyama



Christpher Peck



Keiichi Sasaki



Michael V. Swain



Qing Li



## **Author Contributions**

(1) the conception and design of the study, or acquisition of data, or analysis and interpretation of data: NY KZ SK KS MS QL.

(2) drafting the article or revising it critically for important intellectual content: NY KZ JC ZL CP KS MS QL.

(3) final approval of the version to be submitted: NY KZ JC ZL SK CP KS MS QL.

Manuscript Number MEP-D-17-00459

**Point-by-point responses to the reviewers' comments on the manuscript**

**Article Title: Biomechanical Analysis of Bone Remodeling Following Mandibular Reconstruction using Fibula Free Flap**

Dear Editors and Reviewers,

We wish to thank you and expert reviewers for providing the very constructive comments and insightful suggestions on our manuscript. They have helped greatly enhance our manuscript. By closely following your suggestions and incorporating extra information, we hope that the revised manuscript meets the standard of publication for *Medical Engineering & Physics*.

We hope our dedicated revision have addressed all of your concerns. A detailed point-by-point response is provided as follows.

We look forward to hearing from you again at your earliest convenience.

Yours sincerely,

Nobuhiro Yoda, DDS, PhD.



## Biomechanical Analysis of Bone Remodeling Following Mandibular Reconstruction using Fibula Free Flap

### Highlights

- The longitudinal changes in bone morphology and mineral density systematically in the course of healing/remodeling after mandibular reconstruction with fibula free flap were quantified;
- The mutual influence between the changes in tissue conditions and mandibular mechanobiology by establishing a combined *in-vivo* and *in-silico* approach was assessed for the first time;
- Novel understanding of mechanobiological responses in a healing and remodeling of mandible following mandibular reconstruction was provided.

1           Biomechanical Analysis of Bone Remodeling Following  
2           Mandibular Reconstruction using Fibula Free Flap

3  
4 Nobuhiro Yoda\*<sup>1,2</sup>, Keke Zheng<sup>2</sup>, Junning Chen<sup>3</sup>, Zhipeng Liao<sup>2</sup>, Shigeto Koyama<sup>4</sup>,  
5 Christopher Peck<sup>5</sup>, Michael Swain<sup>6</sup>, Keiichi Sasaki<sup>1</sup>, and Qing Li<sup>2</sup>.

6  
7 <sup>1</sup>Division of Advanced Prosthetic Dentistry, Tohoku University Graduate School of  
8 Dentistry, 4-1, Seiryomachi, Aoba-ku, Sendai, Miyagi, 9808575, Japan

9 <sup>2</sup>School of Aerospace, Mechanical and Mechatronic Engineering, The University of  
10 Sydney, NSW 2006, Australia

11 <sup>3</sup>Department of Biomaterials, Max Planck Institute of Colloids and Interfaces, Am  
12 Mühlenberg 1 OT Golm, 14476 Potsdam, Germany

13 <sup>4</sup>Maxillofacial Prosthetics Clinic, Tohoku University Hospital, 1-1, Seiryomachi, Aoba-  
14 ku, Sendai, Miyagi, 9808575, Japan

15 <sup>5</sup>Faculty of Dentistry, The University of Sydney, Sydney, NSW, 2006, Australia

16 <sup>6</sup>Department of Bioclinical Sciences, Faculty of Dentistry, Kuwait University, Safat  
17 13110, Kuwait

18  
19 **\* Corresponding Author: Nobuhiro Yoda**

20 **Contact details:**

21 Address: Division of Advanced Prosthetic Dentistry, Tohoku University Graduate  
22 School of Dentistry, 4-1, Seiryomachi, Aoba-ku, Sendai, Miyagi, 9808575, JAPAN

23 Phone: +81-22-717-8369; Fax: +81-22-717-8371;

24 E-mail: nobuhiro.yoda.e2@tohoku.ac.jp

## 25 **Abstract**

26 Whilst the newly established biomechanical conditions following mandibular  
27 reconstruction using fibula free flap can be a critical determinant for achieving  
28 favorable bone union, little has been known about their association in a time-dependent  
29 fashion. This study evaluated the bone healing/remodeling activity in reconstructed  
30 mandible and its influence on jaw biomechanics using CT data, and further quantified  
31 their correlation with mechanobiological responses through an *in-silico* approach. A 66-  
32 year-old male patient received mandibular reconstruction was studied. Post-operative  
33 CT scans were taken at 0, 4, 16 and 28 months. Longitudinal change of bone  
34 morphologies and mineral densities were measured at three bone union interfaces (two  
35 between the fibula and mandibular bones and one between the osteotomized fibulas) to  
36 investigate bone healing/remodeling events. Three-dimensional finite element models  
37 were created to quantify mechanobiological responses in the bone at these different time  
38 points. Bone mineral density increased rapidly along the bone interfaces over the first  
39 four months. Cortical bridging formed at the osteotomized interface earlier than the  
40 other two interfaces with larger shape discrepancy between fibula and mandibular bones.  
41 Bone morphology significantly affected mechanobiological responses in the  
42 osteotomized region ( $R^2 > 0.77$ ). The anatomic position and shape discrepancy at bone  
43 union affected the bone healing/remodeling process.

44

45 **Keywords:** Fibula free flap; Finite element analysis; Jaw biomechanics; Mandibular  
46 reconstruction; Bone remodeling.

47



## 48 **1. Introduction**

49 Free vascularized osteocutaneous tissue transfer has become a well-established  
50 procedure for maxillomandibular reconstruction following large resection due to trauma,  
51 atrophy, and tumors ablation [1,2]. Fibula free flap (FFF) provides superior length and  
52 long vascular pedicles for mandibular reconstruction, with proven subsequent high  
53 reliability and adaptability [3]. Nevertheless, some clinical complications remain with  
54 delayed or poor union between the grafted fibula bone and host native mandible [4,5].  
55 Recent CT evaluations reported 20% [6] and 9% [7] non-union rates, respectively. Bone  
56 union determines the strength and health of the reconstructed mandible, both of which  
57 are essential for further occlusal and prosthetic rehabilitation. In the case of bone  
58 fracture healing, the mechanobiological environment, which is thought to regulate  
59 cellular behaviors, can be a critical determinant [8].

60 Unlike general bone fracture healing processes, FFF mandibular reconstruction  
61 may be affected by additional factors, such as shape discrepancy between different  
62 bones and poor bone vascularity [4,9]. Further, the loss of several masticatory muscles  
63 due to resection can cause unbalanced jaw movement and abnormal mastication, leading  
64 to significant change in the biomechanical conditions [10,11]. Thus the  
65 mechanobiological responses in the jaw can be altered significantly; and such a change  
66 in-turn affects subsequent bone remodeling activities [12,13]. To assist surgical planning  
67 and oral rehabilitation it is essential to understand bone healing/remodeling activity and  
68 its influence on jaw biomechanics, thereby preventing delayed or poor union of bone  
69 grafts.

70 Finite element (FE) analysis has the adequacy for the biomechanical studies on

71 orthopaedic [14-16] and dental problems [17-19]. Several those studies demonstrated  
72 their compelling advantages for understanding the biomechanics and mechanobiology  
73 of reconstructed mandibles *in-silico* [20,21]. With recent advances in micro  
74 computerized tomography (CT), bone mineral density (BMD) and morphological  
75 changes can be measured to evaluate bone remodeling sequences noninvasively  
76 [13,22,23]. The CT-based 3D FE models can be thus created to quantify biomechanical  
77 responses to functional forces in a patient-specific and time-dependent manner [24,25].

78         This study aims to (1) examine longitudinal changes in bone morphology and  
79 mineral density in the course of healing/remodeling after mandibular reconstruction  
80 with FFF; and (2) investigate the associated variation in mandibular biomechanics in  
81 terms of mechanical stimulus. The postoperative CT scans were performed at 4 critical  
82 time points over two and half years' clinical follow-up, and the CT images were  
83 segmented for both 2D multiple planar reconstructions (MPR) and 3D (volumetric)  
84 analyses. The bone condition was analyzed in both spatial and temporal manner, in  
85 terms of morphology and BMD. Nonlinear 3D FE analyses were conducted to quantify  
86 the bone mechanobiological stimuli at these different time points; and then correlated to  
87 the corresponding *in-vivo* clinical data. By establishing this combined *in-vivo* and *in-*  
88 *silico* approach, the mutual influence between tissue conditions and mandibular  
89 mechanobiology was assessed. The results are expected to provide important insights  
90 into surgical plan for mandibular reconstruction.

## 91 **2. Materials and Methods**

### 92 ***2.1 Clinical Treatment***

93         A 66-year-old male patient received mandibular reconstruction with

94 osteotomized FFF, due to a squamous-cell carcinoma at the right molar gingiva at the  
95 Department of Otolaryngology-Head and Neck Surgery, Tohoku University Hospital in  
96 Japan. Upon harvesting, the fibular bone was segmented to match the defect jaw  
97 morphology. A titanium fixation plate (Synthes, Solothurn, Switzerland), which was  
98 pre-bent using the CT-based 3D patient model before surgery, was configured to be  
99 fixed monocortically with a total of 11 titanium screws (Synthes, Solothurn,  
100 Switzerland) as shown in Fig. 1. The first CT scan (M0) was performed at the end of  
101 surgery, and the follow-up CTs were taken at 4, 16 and 28 months after surgery (namely,  
102 M4, M16, and M28, respectively). A removable partial denture was inserted into this  
103 subject 6 months after the surgery; however, the subject did not use it for mastication,  
104 due to fear of biting on the reconstructed side. The periodontal conditions of the  
105 remaining teeth and the removable partial denture have been maintained at the  
106 Maxillofacial Prosthetics Clinic in Tohoku University Hospital every three months.

## 107 ***2.2 CT Imaging Acquisition and 2D Image Analysis***

108 Multi-detector helical CT scans were performed for the follow-up examinations  
109 using Somatom Emotion 6 (Siemens, Erlangen, Germany) at 120 kV and 80 mA with  
110 the spatial resolution of 0.4, 0.4, and 0.8 mm in the radial, tangential, and axial  
111 directions. The CT data was further processed with the medical image viewer software  
112 (EV Insite S, PSP Co., Tokyo, Japan), for the detection and alignment of anatomic  
113 landmarks between the different cross-sectional examinations. The mandibular plane  
114 was defined using three reference points; namely, left Gonion point, Menton point, and  
115 inflection point of a titanium fixation plate (green triangles in Fig. 2a). Six planes  
116 parallel to this mandibular plane were selected for the quantitative analysis of bone  
117 union at three docking sites (DS1, DS2, and DS3, respectively) with 2 mm intervals by

118 multiple planar reconstructions (MPR) (Fig. 2b) [12]. On each plane, a 2 mm<sup>3</sup> volume  
119 of interest (VOI) was considered along the superior-inferior axis (Fig. 2b). Since a  
120 significant correlation between Hounsfield units (HU) obtained from clinical CT scans  
121 and bone mineral density (BMD) were established [26], the HU values change in VOIs  
122 can be regarded as the BMD changes over time here, particularly for bone unification at  
123 the contact interfaces. All the VOIs were placed at the same positions throughout these  
124 four time points, based on the distance from the titanium fixation plate and screws as a  
125 reference.

### 126 ***2.3 3D Registration and Volumetric Analysis***

127 3D registration was carried out for investigating the longitudinal changes in  
128 bone surface profile and mineral density using Amira 2016.22 (Zuse Institute Berlin  
129 (ZIB), Berlin, Germany) (Fig. 3a). The titanium fixation plate was selected as the  
130 reference geometry for its rigidity and high contrast. To quantify the variation of BMD  
131 at the docking sites, the change in greyscale was correlated with the distance from the  
132 inferior to the superior aspect. The average value of the pixel intensity (i.e. greyscale)  
133 was calculated in the cortical bone region on each slice (at a regular spacing of 0.8 mm  
134 along the coronal axis), enabling a plot of pixel value change along the axial direction.  
135 To determine the HU values of the cortical bone, several profile lines were constructed  
136 at the CT images cross the region of mature cortical bone. By sampling the histogram  
137 distribution, a HU value of 1536 was determined to be a threshold for determining  
138 cortical bone pixels, which is consistent with the reported HU value of cortical bone for  
139 cone beam CT in literature [27]. By using this cortical bone threshold, variation in both  
140 bone density and volume at the same region for the four time points were quantified.  
141 The detailed variation in bone volume (i.e. volume of the cortical bone voxel cuboids)

142 along this direction was plotted using the same approach. In addition, the variation in  
143 pixel number, rather than the pixel intensity, in the cortical bone region was considered.

#### 144 *2.4 Finite Element Analysis*

145 Four case-specific FE models were created based on the CT data taken at M0,  
146 M4, M16, and M28, respectively [28,29]. The CT images were imported into ScanIP  
147 Ver. 4.3 (Simpleware Ltd, Exeter, UK) for segmentation. The segmented masks (bone,  
148 individual tooth and titanium fixation plate) were further processed in Rhinoceros 4.0  
149 (Robert McNeel & Associates, Seattle, USA) to create parametric models with non-  
150 uniform rational B-spline (NURBS) (Fig. 3b). Following the development of the  
151 mandibular models, the total 11 fixation screws were modeled according to the  
152 manufacturing specifications in Solidworks 2013 (SolidWorks Corp, Waltham, MA,  
153 USA). Those screws were virtually inserted into the models in Rhinoceros 4.0 as guided  
154 by the CT images. Considering that the patient disuse the denture in his daily life and  
155 has no parafunctional habit, the denture was not inserted in the models. To ensure the  
156 numerical accuracy, an adaptive mesh was generated based on a mesh convergence test.  
157 Ten-node quadratic tetrahedral elements with hybrid formulation (C3D10H) were  
158 adopted to ensure smoothness along the contact interfaces.

159 A pixel-based mapping algorithm was adopted to create the heterogeneous bone  
160 density distributions at the different time points, reflecting the changes of the  
161 anatomical conditions [29]. A homogeneous isotropic linear-elastic model was used to  
162 define the teeth (Young's modulus  $E = 20,000$  MPa, Poisson's ratio  $\nu = 0.2$ ), titanium  
163 fixation plates and screws (Ti6Al7Nb:  $E = 110,000$  MPa,  $\nu = 0.3$ ) [21,30].

164 The hinge constraints were prescribed for the corresponding mandibular  
165 condyles. In this subject, the large bone resection was accompanied by the functional

166 loss of the right masseter, medial pterygoid and temporalis muscles; and consequently  
167 masticatory conditions changed dramatically post-surgery. Due to lack of information  
168 regarding muscular forces after such a large resection [20], the magnitudes and  
169 directions of individual forces were derived based on the literature for the remaining  
170 muscles (masseter muscle: 59.23 N, medial pterygoid muscle: 39.60 N, lateral pterygoid  
171 muscle: 34.44 N, and temporalis: 34.09 N, respectively) [31].

172 Strain energy density (SED) was quantified as a mechanobiological stimulus to  
173 analyze the bone responses in the three docking sites and VOIs. SED has been  
174 considered an effective stimulus to bone remodeling in long bones [32] and mandible  
175 [24,33] and can be a scalar quantity to combine stress and strain but eliminate their  
176 directionalities [34]. The SEDs at different time points were correlated with the  
177 corresponding change in the bone density. In this study, linear regression analysis was  
178 performed using IBM SPSS Statistics Ver. 21.0 (IBM Corp., New York, NY, USA) to  
179 examine the correlations between stimuli and bone remodeling progression in all VOIs.  
180 The  $R^2$  values presented the goodness of fit for the predictor functions, thereby  
181 indicating the extent of correlation.

## 182 **3. Results**

### 183 ***3.1 MPR Image Assessment for Bone Morphology and Mineral Density***

184 Fig. 4 shows the longitudinal changes in bone profile from the CT-based MPR  
185 images. In docking site DS1, a significant amount of callus bone formed at time point  
186 M4, and the cortical bridging successfully formed in both buccal and lingual regions at  
187 M16. In DS2, the cortical bridging formed at M4 in both the buccal and lingual regions.  
188 Also, the cortical-like bone appeared to fill the entire interface, while some resorption

189 occurred at the upper and bottom surfaces of cortical bone. In DS3, there was large  
190 discrepancy of bone shape at the initial stage. However, the bone shapes gradually  
191 remodeled and cortical bridging was found in both the buccal and lingual regions at  
192 M16.

193 Fig. 5 shows that the averaged HU value was calculated for each VOI to  
194 quantify the change of BMD. For DS1, both superior and inferior cortical bones  
195 underwent resorption from M0 to M16, while the BMD peaked in the trabecular  
196 interface regions at M4 before undergoing resorption. In contrast, the grafted bones at  
197 DS2 performed exceedingly well in terms of new bone formation, despite being  
198 osteotomized, seen in rapid increases of BMD in the first four months. For DS3, the  
199 cancellous/trabecular region underwent much more dramatic remodeling than the  
200 cortical bone with rapid increase in BMD from M0 to M4 but decrease from M4 to M16.

### 201 ***3.2 Volumetric Assessment of Bone Mineral Density and Morphology***

202 Bone morphological changes were visualized as the apposition and resorption on  
203 the bone surface by 3D volumetric registration in the three docking sites (Fig. 6). The  
204 longitudinal changes in bone volume were site-specific and the rate of volume increase  
205 in the cortical bone region was positive in all the three sites from M4 to M16 (Fig. 7a).  
206 Fig. 7b exhibits the longitudinal change rate of bone volume at each docking site. Bone  
207 volume increased remarkably from M4 to M16 due to new bone formation, especially at  
208 the region from 15 mm to 25 mm for DS1 and from 20 mm to 30 mm for DS3 on the  
209 sectional plane of mandible as visualized in Fig. 6. Fig. 7c plotted the site-specific  
210 change rate of BMD based on the average grayscale in the cortical bone region. Note  
211 that the BMD decreased in the first four months for all the docking sites.

### 212 **3.3 Mechanobiological Stimulus Distribution**

213 Fig. 8 shows the longitudinal changes in the SED distribution and corresponding  
214 CT MPR images of the reconstructed mandible. Both global and local SED distributions  
215 changed with time significantly. The longitudinal changes in morphology and BMD  
216 were remarkable particularly for DS1, leading to substantial variation in the SED  
217 distribution.

218 The SED at VOIs in the cortical bone region was generally higher than that in  
219 the cancellous region in DS1 and DS2 (Fig. 9). At each VOI, the SED decreased with  
220 time at DS1 and DS3, especially in the superior region of DS1. While the increase in  
221 SED with time could be found in some VOIs, the SED dropped from M0 to M4 and  
222 then gradually increased till M28 (but never exceeds that at M0), at 6, 8, and 10 mm  
223 VOIs in DS2.

224 Linear regression analysis between the HU values and SED in VOIs indicated  
225 that there was a strong dependence on the HU values only in DS2 ( $p < 0.05$ ), as shown in  
226 Fig. 10.

## 227 **4. Discussion**

228 Both 2D MPR images and 3D volumetric analyses enabled to quantify and  
229 visualize time-dependent bone apposition and resorption in terms of morphology and  
230 BMD in this FFF reconstructive mandible. This study is believed to be the first of its  
231 kind for investigating the anatomical sequence of healing/remodeling process and its  
232 correlation with mechanobiological responses in a reconstructive mandible.

233 The clinical process of cortical bridging at bone docking regions was found to be



234 significantly site-specific based on the results of both 2D MPR images and 3D  
235 volumetric analyses. Biological healing at bone union is influenced by complex cellular  
236 and molecular activities, and can be affected by the dimension of bone segment gap [35]  
237 and contact shape [9]. In this study, we set up a criterion to justify the cortical bridging,  
238 namely, no gap was observed between the two bones in the six cross sectional planes as  
239 shown in Fig. 4. According to this criterion, the contact region in DS2 achieved earlier  
240 cortical bridging than the other two sites.

241         The BMD became higher within the first four months in all the VOIs except for  
242 the cortical bone regions in DS1 (Fig. 5). Those cortical regions appeared to undergo  
243 significant resorption, while the osseous callus was generally found at the interface of  
244 trabecular regions during the bone-healing phase [36,37]. The BMDs of all the cortical  
245 bone regions in the docking sites were also found to decrease in the first four months,  
246 which was most remarkable for DS2 (Fig. 7c). Despite a vascularized bone graft, the  
247 lower bone vascularity may have caused the reduction of BMD on the cortical region of  
248 the fibula graft [38,39]. Despite the lowered BMD, 3D volumetric analysis revealed a  
249 higher increase rate of bone volume in DS1 than the other two sites over the same time  
250 period (Fig. 7a). Primary bone apposition may have developed throughout formation of  
251 the osseous callus at the endochondral and periosteal areas (Figs. 4 and 5) [35]. The  
252 woven bone with low BMD appears to initially form for filling the gap and reducing  
253 morphological discrepancy, which may be related to the initial volume increase in DS1.  
254 Lamellae bone with high BMD appears to form after M4 [37]. Lower bone vascularity  
255 in the distal segment of osteotomy [39] may limit those biological healing activities in  
256 DS2 and DS3 compared to DS1, further contributing to the initial reduction in the bone  
257 volume (Fig. 7a).

258           Considering the positive increase rates attributable to bone apposition at all three  
259 docking sites from M4 to M16, bone (re)modeling activity had a primary effect on post-  
260 healing bone formation [40,41]. Osseous callus at the interface regions in DS1 and DS3  
261 gradually became cancellous bone, forming a natural mandibular structure during the  
262 course. Nevertheless, the healing and remodeling process at the docking site, especially  
263 with large shape discrepancy, is considered to be significantly slower than those of the  
264 general bone fracture [37,42]. Note that the mandible can be distorted during daily oral  
265 function [43]. Despite the mechanical fixation by titanium plate, the distortion can affect  
266 the mechanical stability of the docking sites, which might also delay the healing process  
267 [9].

268           Mechanical loading is known to stimulate bone healing and remodeling process,  
269 likely enhancing bone mass and functionality [40]. The mechanobiological impetus can  
270 thus be related to the bone remodeling activity [12,13]. SED has been considered an  
271 effective stimulus to bone remodeling in long bones [32] as well as mandible [24,33].  
272 This study revealed the correlation between SED and healing/remodeling outcome over  
273 the time period concerned.

274           The variation in SED distribution was attributed to the time longitudinal change  
275 in the mandibular morphology (Figs. 8 and 9), as well as load transfer in the  
276 restructured mandible, particularly through the fibula grafts. In other words, the  
277 functional load was initially transferred to the fibula graft completely via the titanium  
278 fixation plate (M0); but subsequently, a greater proportion of load transferred through  
279 the bony tissue as the extent of bone union increased. In addition, the remaining  
280 unbalanced muscle activities readapt with time [10,11]. All these factors have a  
281 collective effect on the mechanobiological responses.

282 As shown in Fig. 10, the SED had a strong dependence on the HU values in DS2  
283 ( $p < 0.05$ ). The HU value altered the load bearing capability of the fibula bone, meaning  
284 that the SED is associated with HU values. Lower bone vascularity and good bone  
285 contact condition at DS2 possibly enhance the effect of mechanobiological stimuli on  
286 BMD adaptation, which might be related to the earlier process of cortical bridging at the  
287 DS2. For DS1 and DS3, significant shape discrepancy due to reconstruction generated  
288 non-physiological stress/strain concentration, which might have distorted the  
289 distribution of SED and its correlation to remodeling.

290 Clinically, the implant-supported denture is considered as the most suitable  
291 option for functional rehabilitation following mandibular reconstruction [2]. Although  
292 the timing of implant placement is still controversial, several studies adopted the time  
293 for implant placement at least 6-12 months after the reconstruction with FFF [1,44,45].  
294 Considering the cortical bridging as a predictor of bone union strength [7,46], all the  
295 bone unions can be confirmed through CT scanning, especially in the cases with a large  
296 bone discrepancy. Specifically, favorable initial bone contacts with small shape  
297 discrepancy are considered a primary factor for earlier success of cortical bridging.

298 There are still some limitations in this study. Constrained by the clinical protocol  
299 and radiation dosage allowance, the scanning resolution of CTs could have affected  
300 modeling accuracy. The FE analyses still included several assumptions, such as  
301 simulation under static loading conditions and rotational movement on the mandibular  
302 condyles. The applied muscle forces did not precisely reflect specific condition of this  
303 subject; plus the muscle forces are anticipated to change over time after reconstruction  
304 [47,48]. Consequently, the resultant reaction responses on both temporomandibular  
305 joints might become asymmetric and physiologically complicated. Finally, while the

306 study was featured as patient-specific, the results were based on only one particular  
307 subject. In addition, other patient's factors, such as the systematic background and the  
308 treatment process, could be generally the decisive factors to the bone healing and  
309 remodeling process at the docking sites. Further evaluation and data acquisition of other  
310 subjects with inevitably varied conditions are necessary before generalizing these  
311 clinical and biomechanical findings.

## 312 **5. Conclusion**

313 This newly developed analysis procedure provided a quantitative clinical follow-  
314 up of mandibular reconstruction with fibula free flap (FFF) and fundamental  
315 understanding of time-dependent biomechanical responses in the reconstructed  
316 mandible. It was found that the bone healing and remodeling process at the docking  
317 sites were site-specific; and cortical bridging in the osteotomized region took place  
318 faster than that in the other docking sites between mandibular and fibula bones for the  
319 specific patient concerned. Within the limitation of this study, the anatomic position and  
320 the discrepancy of initial shape at the docking sites between the host mandible and  
321 fibula graft affected the bone healing and remodeling process. It divulged a correlation  
322 between mechanobiological stimulus (strain energy density - SED) and the longitudinal  
323 change in bone mineral density (BMD) and morphology, especially at the osteotomized  
324 region. The longitudinal CT data and mechanobiological correlation generated in this  
325 study provided new insights into patient-specific surgical planning and occlusal  
326 rehabilitation.

327

328 **Conflict of interests**

329 None declared.

330

331 **Ethical approval**

332 The research protocol was approved by the research ethics committee of the Tohoku  
333 University Graduate School of Dentistry (reference #24-10). Full written informed  
334 consent was obtained to use the CT images for this study. All procedures performed in  
335 this study were in accordance with the ethical standards of the 1964 Helsinki  
336 Declaration (<http://www.wma.net>) and its later amendments.

337

338 **Acknowledgements**

339 This work was supported by the Australian Research Council (ARC) through the  
340 Discovery and Fellowship schemes (DP160104602 and FT120100947). We are grateful  
341 to Dr. Atsushi Takeda and Dr. Naoko Sato at Tohoku University Hospital for providing  
342 and caring for this study patient.

343

## 344 **References**

- 345 [1] Hakim SG, Kimmerle H, Trenkle T, Sieg P, Jacobsen HC. Masticatory rehabilitation  
346 following upper and lower jaw reconstruction using vascularised free fibula flap  
347 and enossal implants-19 years of experience with a comprehensive concept. Clin  
348 Oral Invest 2015; 19: 525-34.
- 349 [2] Chiapasco M, Biglioli F, Autelitano L, Romeo E, Brusati R. Clinical outcome of  
350 dental implants placed in fibula-free flaps used for the reconstruction of maxillo-  
351 mandibular defects following ablation for tumors or osteoradionecrosis. Clin Oral  
352 Implants Res 2006; 17: 220-28.
- 353 [3] Hidalgo DA, Rekow AA. Review of 60 consecutive fibula free flap mandible  
354 reconstructions. Plast Reconstr Surg 1995; 96: 585-96.
- 355 [4] Virgin FW, Iseli TA, Iseli CE, Sunde J, Carroll WR, Magnuson JS, Rosenthal EL.  
356 Functional outcomes of fibula and osteocutaneous forearm free flap reconstruction  
357 for segmental mandibular defects. Laryngoscope 2010; 120: 663-7.
- 358 [5] Nam W, Kim HJ, Choi EC, Kim MK, Lee EW, Cha IH. Contributing factors to  
359 mandibulotomy complications: A retrospective study. Oral Surg Oral Med Oral  
360 Pathol Oral Radio Endod 2006; 101: e65-70.
- 361 [6] Yla-Kotola TM, Bartlett E, Goldstein DP, Armstrong K, Gilbert RW, Hofer SOP.  
362 Union and bone resorption of free fibular flaps in mandibular reconstruction. J  
363 Reconstr Microsurg 2013; 29: 427-32.
- 364 [7] Akashi M, Hashikawa K, Kakei Y, Sakakibara A, Hasegawa T, Minamikawa T,  
365 Komori T. Sequential evaluation for bone union of transferred fibula flaps in

- 366 reconstructed mandibles: Panoramic x-ray versus computed tomography. *Int J Oral*  
367 *Maxillofac Surg* 2015; 44: 942-7.
- 368 [8] Gerstenfeld LC, Cullinane DM, Barnes GL, Graves DT, Einhorn TA. Fracture  
369 healing as a post-natal developmental process: Molecular, spatial, and temporal  
370 aspects of its regulation. *J Cell Biochem* 2003; 88: 873-84.
- 371 [9] Feron JM, Mauprivez R. Fracture repair: General aspects and influence of  
372 osteoporosis and anti-osteoporosis treatment. *Injury* 2016; 47 Suppl: 10-4.
- 373 [10] Hannam AG, Stavness IK, Lloyd JE, Fels SS, Miller AJ, Curtis DA. A  
374 comparison of simulated jaw dynamics in models of segmental mandibular  
375 resection versus resection with alloplastic reconstruction. *J Prosthet Dent* 2010;  
376 104: 191-8.
- 377 [11] Namaki S, Morimoto M, Ohba H, Tanaka H, Koshikawa N, Shinohara M.  
378 Masticatory efficiency before and after surgery in oral cancer patients: Comparative  
379 study of glossectomy, marginal mandibulectomy and segmental mandibulectomy. *J*  
380 *Oral Sci* 2004; 46: 113-7.
- 381 [12] Suenaga H, Chen J, Yamaguchi K, Li W, Sasaki K, Swain M, Li Q.  
382 Mechanobiological bone reaction quantified by positron emission tomography. *J*  
383 *Dent Res* 2015; 94: 738-44.
- 384 [13] Chen J, Ahmad R, Suenaga H, Li W, Swain M, Li Q. A comparative study on  
385 complete and implant retained denture treatments - a biomechanics perspective. *J*  
386 *Biomech* 2015; 48: 512-9.
- 387 [14] Mercuri EGF, Daniel AL, Hecke MB, Carvalho L. Influence of different

- 388 mechanical stimuli in a multi-scale mechanobiological isotropic model for bone  
389 remodelling. *Med Eng Phys* 2016; 38: 904-10.
- 390 [15] Yamako G, Chosa E, Zhao X, Totoribe K, Watanabe S, Sakamoto T, Nakane N.  
391 Load-transfer analysis after insertion of cementless anatomical femoral stem using  
392 pre- and post-operative CT images based patient-specific finite element analysis.  
393 *Med Eng Phys* 2016; 36: 694-700.
- 394 [16] Zheng K, Scholes C, Chen J, Parker D, Li Q. Multiobjective optimization of  
395 cartilage stress for non-invasive, patient-specific recommendations of high tibial  
396 osteotomy correction angle. *Med Eng Phys* 2017; 42: 26-34.
- 397 [17] Odin G, Savoldelli C, Bouchard PO, Tillier Y. Determination of Young's  
398 modulus of mandibular bone using inverse analysis. *Med Eng Phys* 2010; 32: 630-  
399 37.
- 400 [18] Bonnet AS, Postaire M, Lipinski P. Biomechanical study of mandible bone  
401 supporting a four-implant retained bridge Finite element analysis of the influence of  
402 bone anisotropy and foodstuff position. *Med Eng Phys* 2009; 31: 806-15.
- 403 [19] Haiat G, Wang HL, Brunski J. Effects of biomechanical properties of the bone-  
404 implant interface on dental implant stability: from in silico approaches to the  
405 patient's mouth. *Annu Rev Biomed Eng* 2014; 16: 187-213.
- 406 [20] Narra N, Valasek J, Hannula M, Marcian P, Sandor GK, Hyttinen J, Wolff J.  
407 Finite element analysis of customized reconstruction plates for mandibular  
408 continuity defect therapy. *J Biomech* 2014; 47: 264-8.
- 409 [21] Tie Y, Wang DM, Ji T, Wang CT, Zhang CP. Three-dimensional finite-element



- 410 analysis investigating the biomechanical effects of human mandibular  
411 reconstruction with autogenous bone grafts. *J Craniomaxillofac Surg* 2006; 34: 290-  
412 8.
- 413 [22] Birkhold AI, Razi H, Weinkamer R, Duda GN, Checa S, Willie BM: Monitoring  
414 in vivo (re)modeling: A computational approach using 4d microct data to quantify  
415 bone surface movements. *Bone* 2015; 75: 210-21.
- 416 [23] Lukas C, Ruffoni D, Lambers FM, Schulte FA, Kuhn G, Kollmannsberger P,  
417 Weinkamer R, Muller R. Mineralization kinetics in murine trabecular bone  
418 quantified by time-lapsed in vivo micro-computed tomography. *Bone* 2013; 56: 55-  
419 60.
- 420 [24] Rungsiyakull C, Chen J, Rungsiyakull P, Li W, Swain M, Li Q. Bone's responses  
421 to different designs of implant-supported fixed partial dentures. *Biomech Model  
422 Mechanobiol* 2015; 14: 403-11.
- 423 [25] C Field, Q Li, W Li, M Thompson, M Swain. Prediction of mandibular bone  
424 remodelling induced by fixed partial dentures. *J Biomech* 2010; 43: 1771-9.
- 425 [26] Schreiber JJ, Anderson PA, Rosas HG, Buchholz AL, Au AG. Hounsfield units  
426 for assessing bone mineral density and strength: A tool for osteoporosis  
427 management. *J Bone Joint Surg* 2011; 93a: 1057-63.
- 428 [27] Reeves TE, Mah P, McDavid WD. Deriving hounsfield units using grey levels in  
429 cone beam CT: a clinical application. *Dentomaxillofac Radiol* 2012; 41: 500-8.
- 430 [28] Yoda N, Liao Z, Chen J, Sasaki K, Swain M, Li Q. Role of implant  
431 configurations supporting three-unit fixedpartial denture on mandibular bone

- 432 response: biological-data-based finite element study. *J Oral Rehabil* 2016; 43: 692-  
433 701.
- 434 [29] Liao Z, Chen J, Zhang Z, Li W, Swain M, Li Q. Computational modeling of  
435 dynamic behaviors of human teeth. *J Biomech* 2015; 48: 4214-20.
- 436 [30] Chen J, Li W, Swain MV, Ali Darendeliler M, Li Q. A periodontal ligament  
437 driven remodeling algorithm for orthodontic tooth movement. *J Biomech* 2014; 47:  
438 1689-95.
- 439 [31] Cruz M, Wassall T, Toledo EM, Barra LP, Lemonge AC. Three-dimensional  
440 finite element stress analysis of a cuneiform-geometry implant. *Int J Oral*  
441 *Maxillofac Implants* 2003; 18: 675-84.
- 442 [32] Huiskes R, Ruimerman R, van Lenthe GH, Janssen JD. Effects of mechanical  
443 forces on maintenance and adaptation of form in trabecular bone. *Nature* 2000; 405:  
444 704-6.
- 445 [33] Lin D, Li Q, Li W, Duckmanton N, Swain M. Mandibular bone remodeling  
446 induced by dental implant. *J Biomech* 2010; 43: 287-93.
- 447 [34] Lin D, Li Q, Li W, Zhou S, Swain MV. Design optimization of functionally  
448 graded dental implant for bone remodeling. *Composites Part B* 2009; 40: 668-75.
- 449 [35] Ai-Aql ZS, Alagl AS, Graves DT, Gerstenfeld LC, Einhorn TA. Molecular  
450 mechanisms controlling bone formation during fracture healing and distraction  
451 osteogenesis. *J Dent Res* 2008; 87: 107-18.
- 452 [36] Vanroermund PM, Romeny BMT, Schoonderwoert GJ, Brandt CJWM,  
453 Sijbrandij S, Renooij W. The use of computed-tomography to quantitate bone-

454 formation after distraction epiphysiolysis in the rabbit. *Skeletal Radiol* 1987; 16:  
455 52-6.

456 [37] Yuasa M, Mignemi NA, Barnett JV, Cates JM, Nyman JS, Okawa A, Yoshii T,  
457 Schwartz HS, Stutz CM, Schoenecker JG. The temporal and spatial development of  
458 vascularity in a healing displaced fracture. *Bone* 2014; 67: 208-21.

459 [38] Jacobsen C, Lubbers HT, Obwegeser J, Soltermann A, Gratz KW. Histological  
460 evaluation of microsurgical revascularized bone in the intraoral cavity: Does it  
461 remain alive? *Microsurgery* 2011; 31: 98-103.

462 [39] Chiodo AA, Gur E, Pang CY, Neligan PC, Boyd JB, Binhammer PM, Forrest  
463 CR. The vascularized pig fibula bone flap model: Effect of segmental osteotomies  
464 and internal fixation on blood flow. *Plast Reconstr Surg* 2000; 105: 1004-12.

465 [40] Birkhold AI, Razi H, Duda GN, Weinkamer R, Checa S, Willie BM. The  
466 influence of age on adaptive bone formation and bone resorption. *Biomaterials*  
467 2014; 35: 9290-301.

468 [41] Christen P, Ito K, Ellouz R, Boutroy S, Sornay-Rendu E, Chapurlat RD, van  
469 Rietbergen B. Bone remodelling in humans is load-driven but not lazy. *Nat*  
470 *Commun* 2014; 5: 4855.

471 [42] Shirota T, Schmelzeisen R, Ohno K, Michi KI. Experimental reconstruction of  
472 mandibular defects with vascularized iliac bone grafts. *J Oral Maxillofac Surg*  
473 1995; 53: 566-71.

474 [43] Koriath TWP, Hannam AG. Deformation of the mandible during simulated tooth  
475 clenching. *J Dent Res* 1994; 73: 56-66.

- 476 [44] Anne-Gaelle B, Samuel S, Julie B, Renaud L, Pierre B. Dental implant  
477 placement after mandibular reconstruction by microvascular free fibula flap:  
478 Current knowledge and remaining questions. *Oral oncol* 2011; 47: 1099-104.
- 479 [45] Chiapasco M, Abati S, Ramundo G, Rossi A, Romeo E, Vogel G. Behavior of  
480 implants in bone grafts or free flaps after tumor resection. *Clin Oral Implants Res*  
481 2000; 11: 66-75.
- 482 [46] Vannabouathong C, Sprague S, Bhandari M. Guidelines for fracture healing  
483 assessments in clinical trials. Part I: Definitions and endpoint committees. *Injury*  
484 2011; 42: 314-6.
- 485 [47] Ishida S, Shibuya Y, Kobayashi M, Komori T. Assessing stomatognathic  
486 performance after mandibulectomy according to the method of mandibular  
487 reconstruction. *Int J Oral Maxillofac Surg* 2015; 44: 948-55.
- 488 [48] Roumanas ED, Garrett N, Blackwell KE, Freymiller E, Abemayor E, Wong WK,  
489 Beumer J, 3rd, Fueki K, Fueki W, Kapur KK. Masticatory and swallowing  
490 threshold performances with conventional and implant-supported prostheses after  
491 mandibular fibula free-flap reconstruction. *J Prosthet Dent* 2006; 96: 289-97.
- 492

1           Biomechanical Analysis of Bone Remodeling Following  
2           Mandibular Reconstruction using Fibula Free Flap  
3

4 Nobuhiro Yoda\*<sup>1,2</sup>, Keke Zheng<sup>2</sup>, Junning Chen<sup>3</sup>, Zhipeng Liao<sup>2</sup>, Shigeto Koyama<sup>4</sup>,  
5 Christopher Peck<sup>5</sup>, Michael Swain<sup>6</sup>, Keiichi Sasaki<sup>1</sup>, and Qing Li<sup>2</sup>.

6  
7 <sup>1</sup>Division of Advanced Prosthetic Dentistry, Tohoku University Graduate School of  
8 Dentistry, 4-1, Seiryomachi, Aoba-ku, Sendai, Miyagi, 9808575, Japan

9 <sup>2</sup>School of Aerospace, Mechanical and Mechatronic Engineering, The University of  
10 Sydney, NSW 2006, Australia

11 <sup>3</sup>Department of Biomaterials, Max Planck Institute of Colloids and Interfaces, Am  
12 Mühlenberg 1 OT Golm, 14476 Potsdam, Germany

13 <sup>4</sup>Maxillofacial Prosthetics Clinic, Tohoku University Hospital, 1-1, Seiryomachi, Aoba-  
14 ku, Sendai, Miyagi, 9808575, Japan

15 <sup>5</sup>Faculty of Dentistry, The University of Sydney, Sydney, NSW, 2006, Australia

16 <sup>6</sup>Department of Bioclinical Sciences, Faculty of Dentistry, Kuwait University, Safat  
17 13110, Kuwait

18  
19 **\* Corresponding Author: Nobuhiro Yoda**

20 **Contact details:**

21 Address: Division of Advanced Prosthetic Dentistry, Tohoku University Graduate  
22 School of Dentistry, 4-1, Seiryomachi, Aoba-ku, Sendai, Miyagi, 9808575, JAPAN

23 Phone: +81-22-717-8369; Fax: +81-22-717-8371;

24 E-mail: nobuhiro.yoda.e2@tohoku.ac.jp

## 25 **Abstract**

26 Whilst the newly established biomechanical conditions following mandibular  
27 reconstruction using fibula free flap can be a critical determinant for achieving  
28 favorable bone union, little has been known about their association in a time-dependent  
29 fashion. This study evaluated the bone healing/remodeling activity in reconstructed  
30 mandible and its influence on jaw biomechanics using CT data, and further quantified  
31 ~~its~~their correlation with mechanobiological responses through an *in-silico* approach. A  
32 66-year-old male patient received mandibular reconstruction was studied. Post-  
33 operative CT scans were taken at 0, 4, 16 and 28 months. Longitudinal change of bone  
34 morphologies and mineral densities were measured at three bone union interfaces (two  
35 between the fibula and mandibular bones and one between the osteotomized fibulas) to  
36 investigate bone healing/remodeling events. Three-dimensional finite element models  
37 were created to quantify mechanobiological responses in the bone at these different time  
38 points. Bone mineral density increased rapidly along the bone interfaces over the first  
39 four months. Cortical bridging formed at the osteotomized interface earlier than the  
40 other two interfaces with larger shape discrepancy between fibula and mandibular bones.  
41 Bone morphology significantly affected mechanobiological responses in the  
42 osteotomized region ( $R^2 > 0.77$ ). The anatomic position and shape discrepancy at bone  
43 union affected the bone healing/remodeling process.

44

45 **Keywords:** Fibula free flap; Finite element analysis; Jaw biomechanics; Mandibular  
46 reconstruction; Bone remodeling.

47

## 48 **1. Introduction**

49 Free vascularized osteocutaneous tissue transfer has become a well-established  
50 procedure for maxillomandibular reconstruction following large resection due to trauma,  
51 atrophy, and tumors ablation [1,2]. Fibula free flap (FFF) provides superior length and  
52 long vascular pedicles for mandibular reconstruction, with proven subsequent high  
53 reliability and adaptability [3]. Nevertheless, some clinical complications remain with  
54 delayed or poor union between the grafted fibula bone and host native mandible [4,5].  
55 Recent CT evaluations reported 20% [6] and 9% [7] non-union rates, respectively. Bone  
56 union determines the strength and health of the reconstructed mandible, both of which  
57 are essential for further ~~bone~~ occlusal and prosthetic rehabilitation. In the case of bone  
58 fracture healing, the mechanobiological environment, which is thought to regulate  
59 cellular behaviors, can be a critical determinant [8].

60 Unlike general bone fracture healing processes, FFF mandibular reconstruction  
61 may be affected by additional factors, such as shape discrepancy between different  
62 bones and poor bone vascularity [4,9]. Further, the loss of several masticatory muscles  
63 due to resection can cause unbalanced jaw movement and abnormal mastication, leading  
64 to significant change in the biomechanical conditions [10,11]. Thus the  
65 mechanobiological responses in the jaw can be altered significantly; and such a change  
66 in-turn affects subsequent bone remodeling activities [12,13]. To assist surgical planning  
67 and oral rehabilitation it is essential to understand bone healing/remodeling activity and  
68 its influence on jaw biomechanics, thereby preventing delayed or poor union of bone  
69 grafts.

70 [Finite element \(FE\) analysis has the adequacy for the biomechanical studies on](#)

71 | orthopaedic [14-16] and dental problems [17-19]. Several those studies demonstrated  
72 | their compelling advantages for understanding the biomechanics and mechanobiology  
73 | of reconstructed mandibles *in-silico* [20,21]. ~~Several finite element (FE) studies~~  
74 | ~~demonstrated their compelling advantages for understanding the biomechanics and~~  
75 | ~~mechanobiology of reconstructed mandibles [14,15].~~ With recent advances in micro  
76 | computerized tomography (CT), bone mineral density (BMD) and morphological  
77 | changes can be measured to evaluate bone remodeling sequences noninvasively  
78 | [~~16,17~~13,22,23]. The CT-based 3D FE models can be thus created to quantify  
79 | biomechanical responses to functional forces in a patient-specific and time-dependent  
80 | manner [~~13,18~~24,25].

81 | This study aims to (1) examine longitudinal changes in bone morphology and  
82 | mineral density in the course of healing/remodeling after mandibular reconstruction  
83 | with FFF; and (2) investigate the associated variation in mandibular biomechanics in  
84 | terms of mechanical stimulus. The postoperative CT scans were performed at 4 critical  
85 | time points over two and half years' clinical follow-up, and the CT images were  
86 | segmented for both 2D multiple planar reconstructions (MPR) and 3D (volumetric)  
87 | analyses. The bone condition was analyzed in both spatial and temporal manner, in  
88 | terms of morphology and BMD. Nonlinear 3D FE analyses were conducted to quantify  
89 | the bone mechanobiological stimuli at the se different time points; and then correlated to  
90 | the corresponding *in-vivo* clinical data. By establishing this combined *in-vivo* and *in-*  
91 | *silico* approach, the mutual influence between tissue conditions and mandibular  
92 | mechanobiology was assessed. The results are expected to provide important insights  
93 | into surgical plan for mandibular reconstruction.



## 94 **2. Materials and Methods**

### 95 ***2.1 Clinical Treatment***

96 A 66-year-old male patient received mandibular reconstruction with  
97 osteotomized FFF, due to a squamous-cell carcinoma at the right molar gingiva at the  
98 Department of Otolaryngology-Head and Neck Surgery, Tohoku University Hospital in  
99 Japan. Upon harvesting, the fibular bone was segmented to match the defect jaw  
100 morphology. A titanium fixation plate (Synthes, Solothurn, Switzerland), which was  
101 pre-bent using the CT-based 3D patient model before surgery, was configured to be  
102 fixed monocortically with a total of 11 titanium screws (Synthes, Solothurn,  
103 Switzerland) as shown in Fig. 1. The first CT scan (M0) was performed at the end of  
104 surgery, and the follow-up CTs were taken at 4, 16 and 28 months after surgery (namely,  
105 M4, M16, and M28, respectively). A removable partial denture was inserted into this  
106 subject 6 months after the surgery; however, the subject did not use it for mastication,  
107 due to fear of biting on the reconstructed side. The periodontal conditions of the  
108 remaining teeth and the removable partial denture have been maintained at the  
109 Maxillofacial Prosthetics Clinic in Tohoku University Hospital every three months.

### 110 ***2.2 CT Imaging Acquisition and 2D Image Analysis***

111 Multi-detector helical CT scans were performed for the follow-up examinations  
112 using Somatom Emotion 6 (Siemens, Erlangen, Germany) at 120 kV and 80 mA with  
113 the spatial resolution of 0.4, 0.4, and 0.8 mm in the radial, tangential, and axial  
114 directions. The CT data was further processed with the medical image viewer software  
115 (EV Insite S, PSP Co., Tokyo, Japan), for the detection and alignment of anatomic  
116 landmarks between the different cross-sectional examinations. The mandibular plane

117 was defined using three reference points; namely, left Gonion point, Menton point, and  
118 inflection point of a titanium fixation plate (green triangles in Fig. 2a). Six planes  
119 parallel to this mandibular plane were selected for the quantitative analysis of bone  
120 union at three docking sites (DS1, DS2, and DS3, respectively) with 2 mm intervals by  
121 multiple planar reconstructions (MPR) (Fig. 2b) [12]. On each plane, a 2 mm<sup>3</sup> volume  
122 of interest (VOI) was ~~placed~~considered along the superior-inferior axis (Fig. 2b). Since  
123 a significant correlation between Hounsfield units (HU) obtained from clinical CT scans  
124 and bone mineral density (BMD) were ~~found~~established [1926], the HU values change  
125 in VOIs can be regarded as the BMD changes over time here, particularly for bone  
126 unification at the contact interfaces. All the VOIs were placed at the same positions  
127 throughout these four time points, based on the distance from the titanium fixation plate  
128 and screws as a reference.

### 129 ***2.3 3D Registration and Volumetric Analysis***

130 3D registration was carried out for investigating the longitudinal changes in  
131 bone surface profile and mineral density using Amira 2016.22 (Zuse Institute Berlin  
132 (ZIB), Berlin, Germany) (Fig. 3a). The titanium fixation plate was selected as the  
133 reference geometry for its rigidity and high contrast. To quantify the variation of BMD  
134 at the docking sites, the change in greyscales was correlated with the distance from the  
135 inferior to the superior aspect. The average value of the pixel intensity (i.e. greyscale)  
136 was calculated in the cortical bone region on each slice (at a regular spacing of 0.8 mm  
137 along the coronal ~~axis~~axial), enabling a plot of pixel value change along the axial direction.  
138 To determine the HU values of the cortical bone, several profile lines were constructed  
139 at the CT images cross the region of mature cortical bone. By sampling the histogram  
140 distribution, a HU value of 1536 was determined to be a threshold for determining

141 | cortical bone pixels, which is ~~in~~-consistent with the reported HU value of cortical bone  
142 | for cone beam CT in literature [2027]. By using this cortical bone threshold, variation in  
143 | both bone density and volume at the same region for the four time points were  
144 | quantified. The detailed variation in bone volume (i.e. volume of the cortical bone voxel  
145 | cuboids) along this direction was plotted using the same approach. In addition, the  
146 | variation in pixel number, rather than the pixel intensity, in the cortical bone region was  
147 | considered.

#### 148 | ***2.4 Finite Element Analysis***

149 | Four case-specific FE models were created based on the CT data taken at M0,  
150 | M4, M16, and M28, respectively [21,22,28,29]. The CT images were imported into  
151 | ScanIP Ver. 4.3 (Simpleware Ltd, Exeter, UK) for segmentation. The segmented masks  
152 | (bone, individual tooth and titanium fixation plate) were further processed in  
153 | Rhinoceros 4.0 (Robert McNeel & Associates, Seattle, USA) to create parametric  
154 | models with non-uniform rational B-spline (NURBS) (Fig. 3b). Following the  
155 | development of the mandibular models, the total 11 fixation screws were modeled  
156 | according to the manufacturing specifications in Solidworks 2013 (SolidWorks Corp,  
157 | Waltham, MA, USA). Those screws were virtually inserted into the models in  
158 | Rhinoceros 4.0 as guided by the CT images. Considering that the patient disuse the  
159 | denture in his daily life and has no parafunctional habit, the denture was not inserted in  
160 | the models. To ensure the numerical accuracy, an adaptive mesh was generated based on  
161 | a mesh convergence test. Ten-node Qquadratic tetrahedral elements with hybrid  
162 | formulation (C3D10H) were adopted to ensure smoothness along the contact interfaces.

163 | A pixel-based mapping algorithm was adopted to create the heterogeneous bone  
164 | density distributions at the different time points, reflecting the changes of the

165 | anatomical conditions [29].<sup>22</sup> A homogeneous isotropic linear-elastic model was used to  
166 | define the teeth (Young's modulus  $E = 20,000$  MPa, Poisson's ratio  $\nu = 0.2$ ), titanium  
167 | fixation plates and screws (Ti6Al7Nb:  $E = 110,000$  MPa,  $\nu = 0.3$ ) [15,23,21,30].

168 |         The hinge constraints were prescribed for the corresponding mandibular  
169 | condyles. In this subject, the large bone resection was accompanied by the functional  
170 | loss of the right masseter, medial pterygoid and temporalis muscles; and consequently  
171 | masticatory conditions changed dramatically post-surgery. Due to lack of information  
172 | regarding muscular forces after such a large resection [420], the magnitudes and  
173 | directions of individual forces were derived based on the literature for the remaining  
174 | muscles (masseter muscle: 59.23 N, medial pterygoid muscle: 39.60 N, lateral pterygoid  
175 | muscle: 34.44 N, and temporalis: 34.09 N, respectively) [2431].

176 |         Strain energy density (SED) was quantified as a mechanobiological stimulus to  
177 | analyze the bone responses in the three docking sites and VOIs. SED has been  
178 | considered an effective stimulus to bone remodeling in long bones [32] and mandible  
179 | [24,33] and can be a scalar quantity to combine stress and strain but eliminate their  
180 | directionalities [34]. The SEDs at different time points were correlated with the  
181 | corresponding change in the bone density. In this study, linear regression analysis was  
182 | performed using IBM SPSS Statistics Ver. 21.0 (IBM Corp., New York, NY, USA) to  
183 | examine the correlations between stimuli and bone remodeling progression in all VOIs.  
184 | The  $R^2$  values presented the goodness of fit for the predictor functions, thereby  
185 | indicating the extent of correlation.

## 186 3. Results

### 187 3.1 MPR Image Assessment for Bone Morphology and Mineral Density

188 Fig. 4 shows the longitudinal changes in bone profile from the CT-based MPR  
189 images. In docking site DS1, a significant amount of callus bone formed at time point  
190 M4, and the cortical bridging successfully formed in both buccal and lingual regions at  
191 M16. In DS2, the cortical bridging formed at M4 in both the buccal and lingual regions.  
192 Also, the cortical-like bone appeared to fill the entire interface, while some resorption  
193 occurred at the upper and bottom surfaces of cortical bone. In DS3, there was large  
194 discrepancy of bone shape at the initial stage. However, the bone shapes gradually  
195 remodeled and cortical bridging was found in both the buccal and lingual regions at  
196 M16.

197 ~~Fig. 5 shows that the averaged HU value was calculated for each VOI to~~  
198 ~~quantify the change of BMD. Averaged HU value was calculated for each VOI to~~  
199 ~~quantify the change of BMD (charts in Fig. 4).~~ For DS1, both superior and inferior  
200 cortical bones underwent resorption from M0 to M16, while the BMD peaked in the  
201 trabecular interface regions at M4 before undergoing resorption. In contrast, the grafted  
202 bones at DS2 performed exceedingly well in terms of new bone formation, despite  
203 being osteotomized, ~~with-seen in~~ rapid increases of BMD in the first four months. For  
204 DS3, the cancellous/trabecular region underwent much more ~~severe-dramatic~~  
205 remodeling than the cortical bone with rapid increase in BMD from M0 to M4 but  
206 decrease from M4 to M16.

207 **3.2 Volumetric Assessment of Bone Mineral Density and Morphology**

208 Bone morphological changes were visualized as the apposition and resorption on  
209 | the bone surface by 3D volumetric registration in the three docking sites (Fig. ~~5a-e~~6).  
210 | The longitudinal changes in bone volume were site-specific and the rate of volume  
211 | increase in the cortical bone region was positive in all the three sites from M4 to M16  
212 | (Fig. ~~5d7a~~). Fig. ~~5e-7b~~ exhibits the longitudinal change rate of bone volume at each  
213 | docking site. Bone volume increased remarkably from M4 to M16 due to new bone  
214 | formation, especially at the region from 15 mm to 25 mm for DS1 and from 20 mm to  
215 | 30 mm for DS3 on the sectional plane of mandible as visualized in Fig. ~~5a-e~~6. Fig. ~~5f-7c~~  
216 | plotted the site-specific change rate of BMD based on the average grayscale in the  
217 | cortical bone region. Note that the BMD decreased in the first four months for all the  
218 | docking sites.

219 **3.3 Mechanobiological Stimulus Distribution**

220 | Fig. ~~6a-8~~ shows the longitudinal changes in the SED distribution and  
221 | corresponding CT MPR images of the reconstructed mandible. Both global and local  
222 | SED distributions changed ~~significantly~~ with time significantly. The longitudinal  
223 | changes in morphology and BMD were remarkable particularly for DS1, leading to  
224 | substantial variation in the SED distribution.

225 The SED at VOIs in the cortical bone region was generally higher than that in  
226 | the cancellous region in DS1 and DS2 (Fig. ~~6b9~~). At each VOI, the SED decreased with  
227 | time at DS1 and DS3, especially in the superior region of DS1. While the increase in  
228 | SED with time could be found in some VOIs, the SED dropped from M0 to M4 and  
229 | then gradually increased till M28 (but never exceeds that at M0), at 6, 8, and 10 mm

230 VOIs in DS2.

231 Linear regression analysis between the HU values and SED in VOIs indicated  
232 that there was a strong dependence on the HU values only in DS2 (p<0.05), as shown in  
233 Fig. 10.

## 234 **4. Discussion**

235 Both 2D MPR images and 3D volumetric analyses enabled to quantify and  
236 visualize time-dependent bone apposition and resorption in terms of morphology and  
237 BMD in this FFF reconstructive mandible. This study is believed to be the first of its  
238 kind for investigating the anatomical sequence of healing/remodeling process and its  
239 correlation with mechanobiological responses in a reconstructive mandible.

240 The clinical process of cortical bridging at bone docking regions was found to be  
241 significantly site-specific based on the results of both 2D MPR images and 3D  
242 volumetric analyses. Biological healing at bone union is influenced by complex cellular  
243 and molecular activities, and can be affected by the dimension of bone segment gap  
244 [2535] and contact shape [9]. In this study, we set up a criterion to justify the cortical  
245 bridging, namely, no gap was observed between the two bones in the six cross sectional  
246 planes as shown in Fig. 4. According to this criterion, the contact region in DS2  
247 achieved earlier cortical bridging than the other two sites. Specifically, the contact region  
248 in DS2 achieved earlier cortical bridging than the other two sites (Fig. 4).

249 The BMD became higher within the first four months in all the VOIs except for  
250 the cortical bone regions in DS1 (Fig. 45). Those cortical regions appeared to undergo  
251 significant resorption, while the osseous callus was generally found at the interface of

252 | trabecular regions during the bone-healing phase [26,2736,37]. The BMDs of all the  
253 | cortical bone regions in the docking sites were also found to decrease in the first four  
254 | months, which was most remarkable for DS2 (Fig. 547c). Despite a vascularized bone  
255 | graft, the lower bone vascularity may have caused the reduction of BMD on the cortical  
256 | region of the fibula graft [28,2938,39]. Despite the lowered BMD, 3D volumetric  
257 | analysis revealed a higher increase rate of bone volume in DS1 than the other two sites  
258 | over the same time period (Fig. 547a). Primary bone apposition may have developed  
259 | throughout formation of the osseous callus at the endochondral and periosteal areas  
260 | (Figs. 4a4 and 5) [2535]. The woven bone with low BMD appears to initially form for  
261 | filling the gap and reducing morphological discrepancy, which may be related to the  
262 | initial volume increase in DS1. Lamellae bone with high BMD appears to form after M4  
263 | [2737]. Lower bone vascularity in the distal segment of osteotomy [2939] may limit  
264 | those biological healing activities in DS2 and DS3 compared to DS1, further  
265 | contributing to the initial reduction in the bone volume (Fig. 547a).

266 |         Considering the positive increase rates attributable to bone apposition at all three  
267 | docking sites from M4 to M16, bone (re)modeling activity had a primary effect on post-  
268 | healing bone formation [30,3140,41]. Osseous callus at the interface regions in DS1 and  
269 | DS3 gradually became cancellous bone, forming a natural mandibular structure during  
270 | the course. Nevertheless, the healing and remodeling process at the docking site,  
271 | especially with large shape discrepancy, is considered to be significantly slower than  
272 | those of the general bone fracture [27,3237,42]. Note that the mandible can be distorted  
273 | during daily oral function [3343]. Despite the mechanical fixation by titanium plate, the  
274 | distortion can affect the mechanical stability of the docking sites, which might also  
275 | delay the healing process [9].



276 Mechanical loading is known to stimulate bone healing and remodeling process,  
277 likely enhancing bone mass and functionality [3040]. The mechanobiological impetus  
278 can thus be related to the bone remodeling activity [12,13]. SED has been considered an  
279 effective stimulus to bone remodeling in long bones [3432] ~~and as well as~~ mandible  
280 [18,3524,33]. This study revealed the correlation between SED and healing/remodeling  
281 outcome over the time period concerned.

282 The variation in SED distribution was attributed to the time longitudinal change  
283 in the mandibular morphology (Figs. 68 and 9), as well as load transfer in the  
284 restructured mandible, particularly through the fibula grafts. In other words, the  
285 functional load was initially transferred to the fibula graft completely via the titanium  
286 fixation plate (M0); but subsequently, a greater proportion of load transferred through  
287 the bony tissue as the extent of bone union increased. In addition, the remaining  
288 unbalanced muscle activities readapt with time [10,11]. All these factors have a  
289 collective effect on the mechanobiological responses.

290 As shown in Fig. 710, the SED had a strong dependence on the HU values in  
291 DS2 ( $p < 0.05$ ). The HU value altered the load bearing capability of the fibula bone,  
292 meaning that the SED is associated with HU values. Lower bone vascularity and good  
293 bone contact condition at DS2 possibly enhance the effect of mechanobiological stimuli  
294 on BMD adaptation, which might be related to the earlier process of cortical bridging at  
295 the DS2. For DS1 and DS3, significant shape discrepancy due to reconstruction  
296 generated non-physiological stress/strain concentration, which might have distorted the  
297 distribution of SED and its correlation to remodeling.

298 Clinically, the implant-supported denture is considered as the most suitable

299 option for functional rehabilitation following mandibular reconstruction [2]. Although  
300 the timing of implant placement is still controversial, several studies adopted the time  
301 for implant placement at least 6–12 months after the reconstruction with FFF  
302 [1,36,37,44,45]. Considering the cortical bridging as a predictor of bone union strength  
303 [7,38,46], all the bone unions can be confirmed through CT scanning, especially in the  
304 cases with a large bone discrepancy. Specifically, favorable initial bone contacts with  
305 small shape discrepancy are considered a primary factor for earlier success of cortical  
306 bridging.

307         There are still some limitations in this study. Constrained by the clinical protocol  
308 and radiation dosage allowance, the scanning resolution of CTs could have affected  
309 modeling accuracy. The FE analyses still included several assumptions, such as  
310 simulation under static loading conditions and rotational movement on the mandibular  
311 condyles. The applied muscle forces did not precisely reflect specific condition of this  
312 subject; plus the muscle forces are anticipated to change over time after reconstruction  
313 [39,40,47,48]. Consequently, the resultant reaction responses on both  
314 temporomandibular joints might become asymmetric and physiologically complicated.  
315 Finally, while the study was featured as patient-specific, the results were based on only  
316 one particular subject. In addition, other patient's factors, such as the systematic  
317 background and the treatment process, could be generally the decisive factors to the  
318 bone healing and remodeling process at the docking sites. Further evaluation and data  
319 acquisition of other subjects with inevitably varied conditions are necessary before  
320 generalizing these clinical and biomechanical findings.

321 **5. Conclusion**

322 | This newly developed ~~analysing methods~~analysis procedure provided a  
323 | quantitative clinical follow-up of mandibular reconstruction with fibula free flap (FFF)  
324 | and fundamental understanding of time-dependent biomechanical responses in the  
325 | reconstructed mandible. It was found that the bone healing and remodeling process at  
326 | the docking sites were site-specific; and cortical bridging in the osteotomized region  
327 | took place faster than that in the other docking sites between mandibular and fibula  
328 | bones for the specific patient concerned. Within the limitation of this study, the  
329 | anatomic position and the discrepancy of initial shape at the docking sites between the  
330 | host mandible and fibula graft affected the bone healing and remodeling process. It  
331 | ~~revealed~~divulged a correlation between mechanobiological stimulus (strain energy  
332 | density - SED) and the longitudinal change in bone mineral density (BMD) and  
333 | morphology, especially at the osteotomized region. The longitudinal CT data and  
334 | mechanobiological correlation generated in this study provided new insights into  
335 | patient-specific surgical planning and occlusal rehabilitation.

336

337 **Conflict of interests**

338 None declared.

339

340 **Ethical approval**

341 The research protocol was approved by the research ethics committee of the Tohoku  
342 University Graduate School of Dentistry (reference #24-10). Full written informed  
343 consent was obtained to use the CT images for this study. All procedures performed in  
344 this study were in accordance with the ethical standards of the 1964 Helsinki  
345 Declaration (<http://www.wma.net>) and its later amendments.

346

347 **Acknowledgements**

348 This work was supported by the Australian Research Council (ARC) through the  
349 Discovery and Fellowship schemes (DP160104602 and FT120100947). We are grateful  
350 to Dr. Atsushi Takeda and Dr. Naoko Sato at Tohoku University Hospital for providing  
351 and caring for this study patient.

352

## 353 **References**

- 354 [1] Hakim SG, Kimmerle H, Trenkle T, Sieg P, Jacobsen HC. Masticatory rehabilitation  
355 following upper and lower jaw reconstruction using vascularised free fibula flap  
356 and enossal implants-19 years of experience with a comprehensive concept. Clin  
357 Oral Invest 2015; 19: 525-34.
- 358 [2] Chiapasco M, Biglioli F, Autelitano L, Romeo E, Brusati R. Clinical outcome of  
359 dental implants placed in fibula-free flaps used for the reconstruction of maxillo-  
360 mandibular defects following ablation for tumors or osteoradionecrosis. Clin Oral  
361 Implants Res 2006; 17: 220-28.
- 362 [3] Hidalgo DA, Rekow AA. Review of 60 consecutive fibula free flap mandible  
363 reconstructions. Plast Reconstr Surg 1995; 96: 585-96.
- 364 [4] Virgin FW, Iseli TA, Iseli CE, Sunde J, Carroll WR, Magnuson JS, Rosenthal EL.  
365 Functional outcomes of fibula and osteocutaneous forearm free flap reconstruction  
366 for segmental mandibular defects. Laryngoscope 2010; 120: 663-7.
- 367 [5] Nam W, Kim HJ, Choi EC, Kim MK, Lee EW, Cha IH. Contributing factors to  
368 mandibulotomy complications: A retrospective study. Oral Surg Oral Med Oral  
369 Pathol Oral Radio Endod 2006; 101: e65-70.
- 370 [6] Yla-Kotola TM, Bartlett E, Goldstein DP, Armstrong K, Gilbert RW, Hofer SOP.  
371 Union and bone resorption of free fibular flaps in mandibular reconstruction. J  
372 Reconstr Microsurg 2013; 29: 427-32.
- 373 [7] Akashi M, Hashikawa K, Kakei Y, Sakakibara A, Hasegawa T, Minamikawa T,  
374 Komori T. Sequential evaluation for bone union of transferred fibula flaps in

- 375 reconstructed mandibles: Panoramic x-ray versus computed tomography. Int J Oral  
376 Maxillofac Surg 2015; 44: 942-7.
- 377 [8] Gerstenfeld LC, Cullinane DM, Barnes GL, Graves DT, Einhorn TA. Fracture  
378 healing as a post-natal developmental process: Molecular, spatial, and temporal  
379 aspects of its regulation. J Cell Biochem 2003; 88: 873-84.
- 380 [9] Feron JM, Mauprivez R. Fracture repair: General aspects and influence of  
381 osteoporosis and anti-osteoporosis treatment. Injury 2016; 47 Suppl: 10-4.
- 382 [10] Hannam AG, Stavness IK, Lloyd JE, Fels SS, Miller AJ, Curtis DA. A  
383 comparison of simulated jaw dynamics in models of segmental mandibular  
384 resection versus resection with alloplastic reconstruction. J Prosthet Dent 2010;  
385 104: 191-8.
- 386 [11] Namaki S, Morimoto M, Ohba H, Tanaka H, Koshikawa N, Shinohara M.  
387 Masticatory efficiency before and after surgery in oral cancer patients: Comparative  
388 study of glossectomy, marginal mandibulectomy and segmental mandibulectomy. J  
389 Oral Sci 2004; 46: 113-7.
- 390 [12] Suenaga H, Chen J, Yamaguchi K, Li W, Sasaki K, Swain M, Li Q.  
391 Mechanobiological bone reaction quantified by positron emission tomography. J  
392 Dent Res 2015; 94: 738-44.
- 393 [13] Chen J, Ahmad R, Suenaga H, Li W, Swain M, Li Q. A comparative study on  
394 complete and implant retained denture treatments - a biomechanics perspective. J  
395 Biomech 2015; 48: 512-9.
- 396 [14] Mercuri EGF, Daniel AL, Hecke MB, Carvalho L. Influence of different

- 397 mechanical stimuli in a multi-scale mechanobiological isotropic model for bone  
398 remodelling. Med Eng Phys 2016; 38: 904-10.
- 399 [15] Yamako G, Chosa E, Zhao X, Totoribe K, Watanabe S, Sakamoto T, Nakane N.  
400 Load-transfer analysis after insertion of cementless anatomical femoral stem using  
401 pre- and post-operative CT images based patient-specific finite element analysis.  
402 Med Eng Phys 2016; 36: 694-700.
- 403 [16] Zheng K, Scholes C, Chen J, Parker D, Li Q. Multiobjective optimization of  
404 cartilage stress for non-invasive, patient-specific recommendations of high tibial  
405 osteotomy correction angle. Med Eng Phys 2017; 42: 26-34.
- 406 [17] Odin G, Savoldelli C, Bouchard PO, Tillier Y. Determination of Young's  
407 modulus of mandibular bone using inverse analysis. Med Eng Phys 2010; 32: 630-  
408 37.
- 409 [18] Bonnet AS, Postaire M, Lipinski P. Biomechanical study of mandible bone  
410 supporting a four-implant retained bridge Finite element analysis of the influence of  
411 bone anisotropy and foodstuff position. Med Eng Phys 2009; 31: 806-15.
- 412 [19] Haiat G, Wang HL, Brunski J. Effects of biomechanical properties of the bone-  
413 implant interface on dental implant stability: from in silico approaches to the  
414 patient's mouth. Annu Rev Biomed Eng 2014; 16: 187-213.
- 415 ~~[13]~~—
- 416 ~~[14]~~[20] Narra N, Valasek J, Hannula M, Marcian P, Sandor GK, Hyttinen J,  
417 Wolff J. Finite element analysis of customized reconstruction plates for mandibular  
418 continuity defect therapy. J Biomech 2014; 47: 264-8.

419 | ~~[15]~~[21] Tie Y, Wang DM, Ji T, Wang CT, Zhang CP. Three-dimensional finite-  
420 | element analysis investigating the biomechanical effects of human mandibular  
421 | reconstruction with autogenous bone grafts. J Craniomaxillofac Surg 2006; 34: 290-  
422 | 8.

423 | ~~[16]~~[22] Birkhold AI, Razi H, Weinkamer R, Duda GN, Checa S, Willie BM:  
424 | Monitoring in vivo (re)modeling: A computational approach using 4d microct data  
425 | to quantify bone surface movements. Bone 2015; 75: 210-21.

426 | ~~[17]~~[23] Lukas C, Ruffoni D, Lambers FM, Schulte FA, Kuhn G,  
427 | Kollmannsberger P, Weinkamer R, Muller R. Mineralization kinetics in murine  
428 | trabecular bone quantified by time-lapsed in vivo micro-computed tomography.  
429 | Bone 2013; 56: 55-60.

430 | [\[24\]](#) Rungsiyakull C, Chen J, Rungsiyakull P, Li W, Swain M, Li Q. Bone's responses  
431 | to different designs of implant-supported fixed partial dentures. Biomech Model  
432 | Mechanobiol 2015; 14: 403-11.

433 | [\[25\]](#) C Field, Q Li, W Li, M Thompson, M Swain. Prediction of mandibular bone  
434 | remodelling induced by fixed partial dentures. J Biomech 2010; 43: 1771-9.

435 | ~~[18]~~—

436 | ~~[19]~~[26] Schreiber JJ, Anderson PA, Rosas HG, Buchholz AL, Au AG. Hounsfield  
437 | units for assessing bone mineral density and strength: A tool for osteoporosis  
438 | management. J Bone Joint Surg 2011; 93a: 1057-63.

439 | ~~[20]~~[27] Reeves TE, Mah P, McDavid WD. Deriving hounsfield units using grey  
440 | levels in cone beam CT: a clinical application. Dentomaxillofac Radiol 2012; 41:



441 500-8.

442 ~~[21]~~~~[28]~~ Yoda N, Liao Z, Chen J, Sasaki K, Swain M, Li Q. Role of implant  
443 configurations supporting three-unit fixedpartial denture on mandibular bone  
444 response: biological-data-based finite element study. J Oral Rehabil 2016; 43: 692-  
445 701.

446 ~~[22]~~~~[29]~~ Liao Z, Chen J, Zhang Z, Li W, Swain M, Li Q. Computational modeling  
447 of dynamic behaviors of human teeth. J Biomech 2015; 48: 4214-20.

448 ~~[23]~~~~[30]~~ Chen J, Li W, Swain MV, Ali Darendeliler M, Li Q. A periodontal  
449 ligament driven remodeling algorithm for orthodontic tooth movement. J Biomech  
450 2014; 47: 1689-95.

451 [\[31\]](#) Cruz M, Wassall T, Toledo EM, Barra LP, Lemonge AC. Three-dimensional  
452 finite element stress analysis of a cuneiform-geometry implant. Int J Oral  
453 Maxillofac Implants 2003; 18: 675-84.

454 [\[32\] Huiskes R, Ruimerman R, van Lenthe GH, Janssen JD. Effects of mechanical  
455 forces on maintenance and adaptation of form in trabecular bone. Nature 2000; 405:  
456 704-6.](#)

457 [\[33\] Lin D, Li Q, Li W, Duckmanton N, Swain M. Mandibular bone remodeling  
458 induced by dental implant. J Biomech 2010; 43: 287-93.](#)

459 [\[34\] Lin D, Li Q, Li W, Zhou S, Swain MV. Design optimization of functionally  
460 graded dental implant for bone remodeling. Composites Part B 2009; 40: 668-75.](#)

461 ~~[24]~~—

462 ~~[25]~~~~[35]~~ Ai-Aql ZS, Alagl AS, Graves DT, Gerstenfeld LC, Einhorn TA.

463 Molecular mechanisms controlling bone formation during fracture healing and  
464 distraction osteogenesis. J Dent Res 2008; 87: 107-18.

465 | ~~[26]~~[36]\_\_\_\_ Vanroermund PM, Romeny BMT, Schoonderwoert GJ, Brandt CJWM,  
466 Sijbrandij S, Renooij W. The use of computed-tomography to quantitate bone-  
467 formation after distraction epiphysiolysis in the rabbit. Skeletal Radiol 1987; 16:  
468 52-6.

469 | ~~[27]~~[37]\_\_\_\_ Yuasa M, Mignemi NA, Barnett JV, Cates JM, Nyman JS, Okawa A,  
470 Yoshii T, Schwartz HS, Stutz CM, Schoenecker JG. The temporal and spatial  
471 development of vascularity in a healing displaced fracture. Bone 2014; 67: 208-21.

472 | ~~[28]~~[38]\_\_\_\_ Jacobsen C, Lubbers HT, Obwegeser J, Soltermann A, Gratz KW.  
473 Histological evaluation of microsurgical revascularized bone in the intraoral cavity:  
474 Does it remain alive? Microsurgery 2011; 31: 98-103.

475 | ~~[29]~~[39]\_\_\_\_ Chiodo AA, Gur E, Pang CY, Neligan PC, Boyd JB, Binhammer PM,  
476 Forrest CR. The vascularized pig fibula bone flap model: Effect of segmental  
477 osteotomies and internal fixation on blood flow. Plast Reconstr Surg 2000; 105:  
478 1004-12.

479 | ~~[30]~~[40]\_\_\_\_ Birkhold AI, Razi H, Duda GN, Weinkamer R, Checa S, Willie BM. The  
480 influence of age on adaptive bone formation and bone resorption. Biomaterials  
481 2014; 35: 9290-301.

482 | ~~[31]~~[41]\_\_\_\_ Christen P, Ito K, Ellouz R, Boutroy S, Sornay-Rendu E, Chapurlat RD,  
483 van Rietbergen B. Bone remodelling in humans is load-driven but not lazy. Nat  
484 Commun 2014; 5: 4855.

485 | ~~[32]~~[42]\_\_\_\_Shirota T, Schmelzeisen R, Ohno K, Michi KI. Experimental  
486 | reconstruction of mandibular defects with vascularized iliac bone grafts. J Oral  
487 | Maxillofac Surg 1995; 53: 566-71.

488 | ~~[33]~~[43]\_\_\_\_Korioth TWP, Hannam AG. Deformation of the mandible during  
489 | simulated tooth clenching. J Dent Res 1994; 73: 56-66.

490 | ~~[34]—Huiskes R, Ruimerman R, van Lenthe GH, Janssen JD. Effects of mechanical  
491 | forces on maintenance and adaptation of form in trabecular bone. Nature 2000; 405:  
492 | 704-6.~~

493 | ~~[35]—Lin D, Li Q, Li W, Duckmanton N, Swain M. Mandibular bone remodeling  
494 | induced by dental implant. J Biomech 2010; 43: 287-93.~~

495 | ~~[36]~~[44]\_\_\_\_Anne-Gaelle B, Samuel S, Julie B, Renaud L, Pierre B. Dental implant  
496 | placement after mandibular reconstruction by microvascular free fibula flap:  
497 | Current knowledge and remaining questions. Oral oncol 2011; 47: 1099-104.

498 | ~~[37]~~[45]\_\_\_\_Chiapasco M, Abati S, Ramundo G, Rossi A, Romeo E, Vogel G.  
499 | Behavior of implants in bone grafts or free flaps after tumor resection. Clin Oral  
500 | Implants Res 2000; 11: 66-75.

501 | ~~[38]~~[46]\_\_\_\_Vannabouathong C, Sprague S, Bhandari M. Guidelines for fracture  
502 | healing assessments in clinical trials. Part I: Definitions and endpoint committees.  
503 | Injury 2011; 42: 314-6.

504 | ~~[39]~~[47]\_\_\_\_Ishida S, Shibuya Y, Kobayashi M, Komori T. Assessing stomatognathic  
505 | performance after mandibulectomy according to the method of mandibular  
506 | reconstruction. Int J Oral Maxillofac Surg 2015; 44: 948-55.

507 | ~~[40]~~[48]\_\_\_\_Roumanas ED, Garrett N, Blackwell KE, Freymiller E, Abemayor E,  
508 | Wong WK, Beumer J, 3rd, Fueki K, Fueki W, Kapur KK. Masticatory and  
509 | swallowing threshold performances with conventional and implant-supported  
510 | prostheses after mandibular fibula free-flap reconstruction. J Prosthet Dent 2006;  
511 | 96: 289-97.  
512 |

## 1 Captions to illustrations

2 **Figure 1. Intraoperative view illustrating the fibula bone affixed to the titanium**  
3 **fixation plate.**

4 White triangle: mandibular bone, Black triangle: fibula bone. **Green arrows: Screw**  
5 **position (8 of 11 screws are shown in this picture).** The flap pedicles were anastomosed  
6 with the thyroid artery and the external jugular vein.

7

8 **Figure 2. Clinical X-ray and CT images for assessment.**

9 (a) Postoperative radiograph (M0). Yellow boxes: three investigated docking sites (DS1,  
10 DS2 and DS3) for the bone union. Green triangles: reference points for defining  
11 mandibular plane for 2D MPR (multiple planar reconstructions) analysis. (b) CT MPR  
12 cross-sectional images of contact interface perpendicular to the mandibular plane (green  
13 line in (b)) at three docking sites at M0; brown: mandible, yellow: anterior fragment of  
14 fibula bone, green: posterior fragment of fibula bone. Lateral lines: planes for analysis,  
15 boxes: cubic (**2 mm<sup>3</sup>**) volume of interests (VOIs).

16

17 **Figure 3. Procedure of 3D image registration and computational model for finite**  
18 **element analysis.**

19 (a) Procedure of 3D image registration for investigating the longitudinal changes in  
20 bone surface profile and mineral density; the example for the DS1 between M0 **model**  
21 **(orange)** and M4 **model (blue)**. Titanium fixation plate was selected as the reference  
22 geometry for the registration. (b) 3D modeling for the patient's jaw model (M0) with

23 non-uniform rational B-spline (NURBS).

24

25 **Figure 4. MPR CT image analysis.**

26 (a) DS 1, (b) DS 2, (c) DS 3. Individual planes and VOIs are defined in **Figure 2**. Each  
27 **plane** position stated in terms of the distance from the bottom. Both top and bottom  
28 planes included the cortical bone region of fibula graft at M0.

29

30 **Figure 5. Time-dependent changes in HU value.**

31 (a) DS 1, (b) DS 2, (c) DS 3.

32

33 **Figure 6. Volumetric analysis of bone morphology changes by 3D image**  
34 **registration and superimposition.**

35 (a) DS 1, (b) DS 2, (c) DS 3

36

37 **Figure 7. Volumetric analysis of bone morphological changes.**

38 (a) Volume increase rate in the cortical bone region, (b) Site-specific volume change  
39 rate (%), (c) Site-specific BMD (greyscale) increase rate (%) based on the grayscale on  
40 the cortical bone region.

41

42 **Figure 8. Mechanobiological stimulus distributions.**

43 (a) M0, (b) M4, (c) M16, (d) M28. SED distribution was shown at the different time

44 points and in different regions along with corresponding CT MPR images (anterior end  
45 of fibula graft in DS1 and posterior end of fibula graft in DS3).

46

47 **Figure 9. Average values of SED in each VOI assigned in the same location as in**  
48 **the CT MPR image.**

49 VOI position stated in terms of the distance from the bottom at each docking site shown  
50 in Fig. 2.

51

52 **Figure 10. Linear regression analysis between CT Hounsfield Unit (HU) and SED**  
53 **in volume of interests (VOIs)**

54 The VOIs were on the same location in each multiple planar reconstruction (MPR)  
55 image at each docking site shown in Fig. 2. \*P < 0.05, \*\*P < 0.01.

Figure 1  
[Click here to download high resolution image](#)

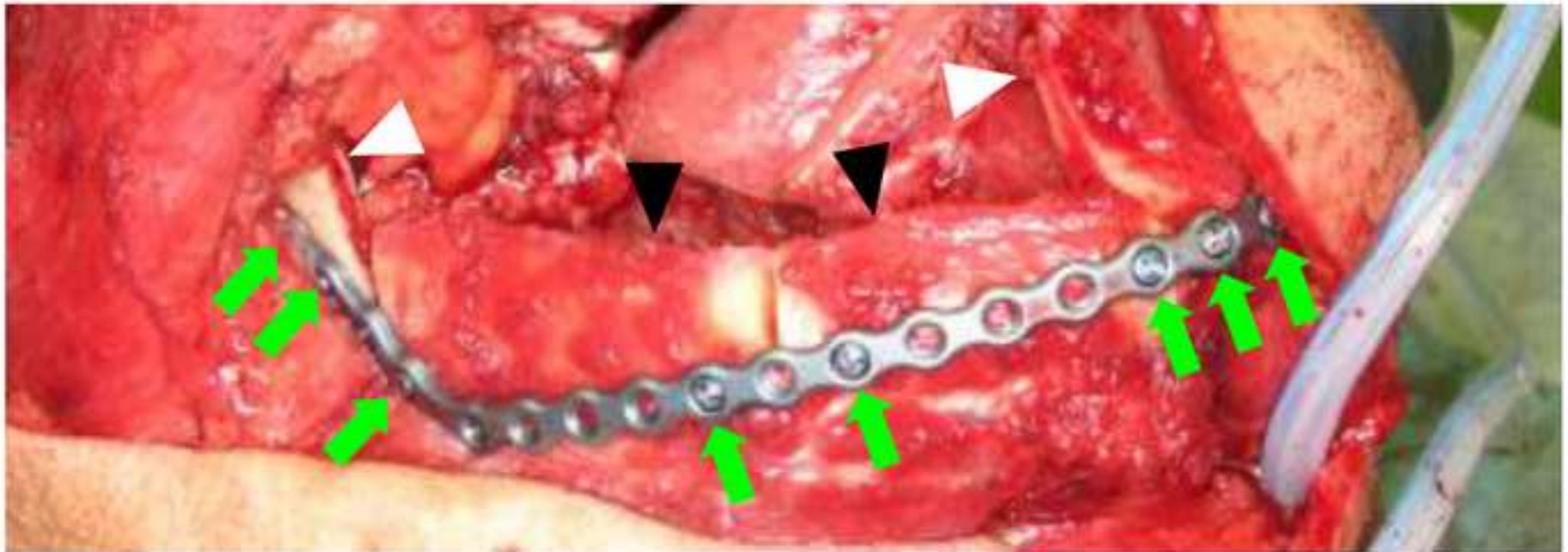
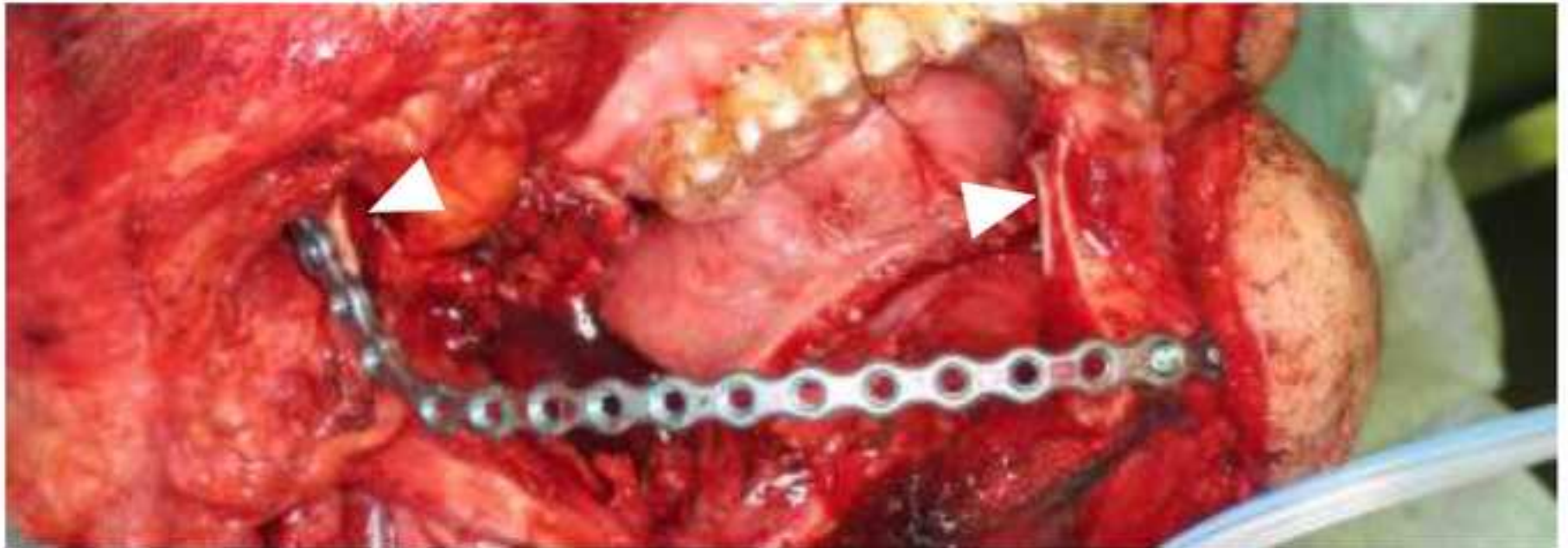




Figure 2  
[Click here to download high resolution image](#)

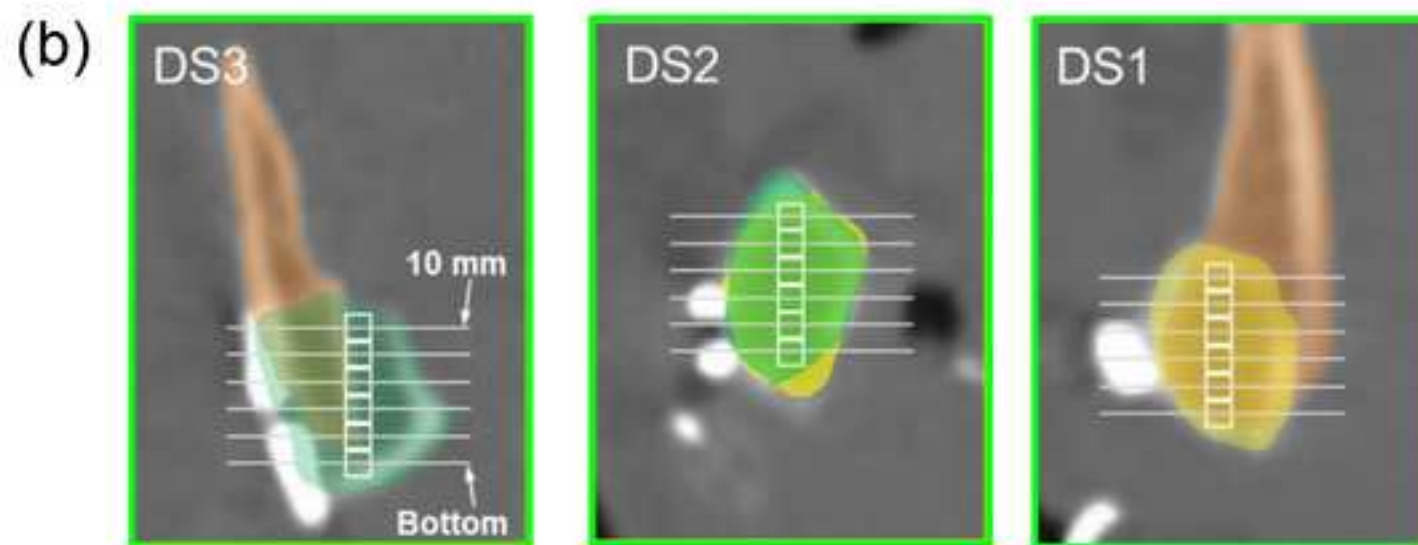
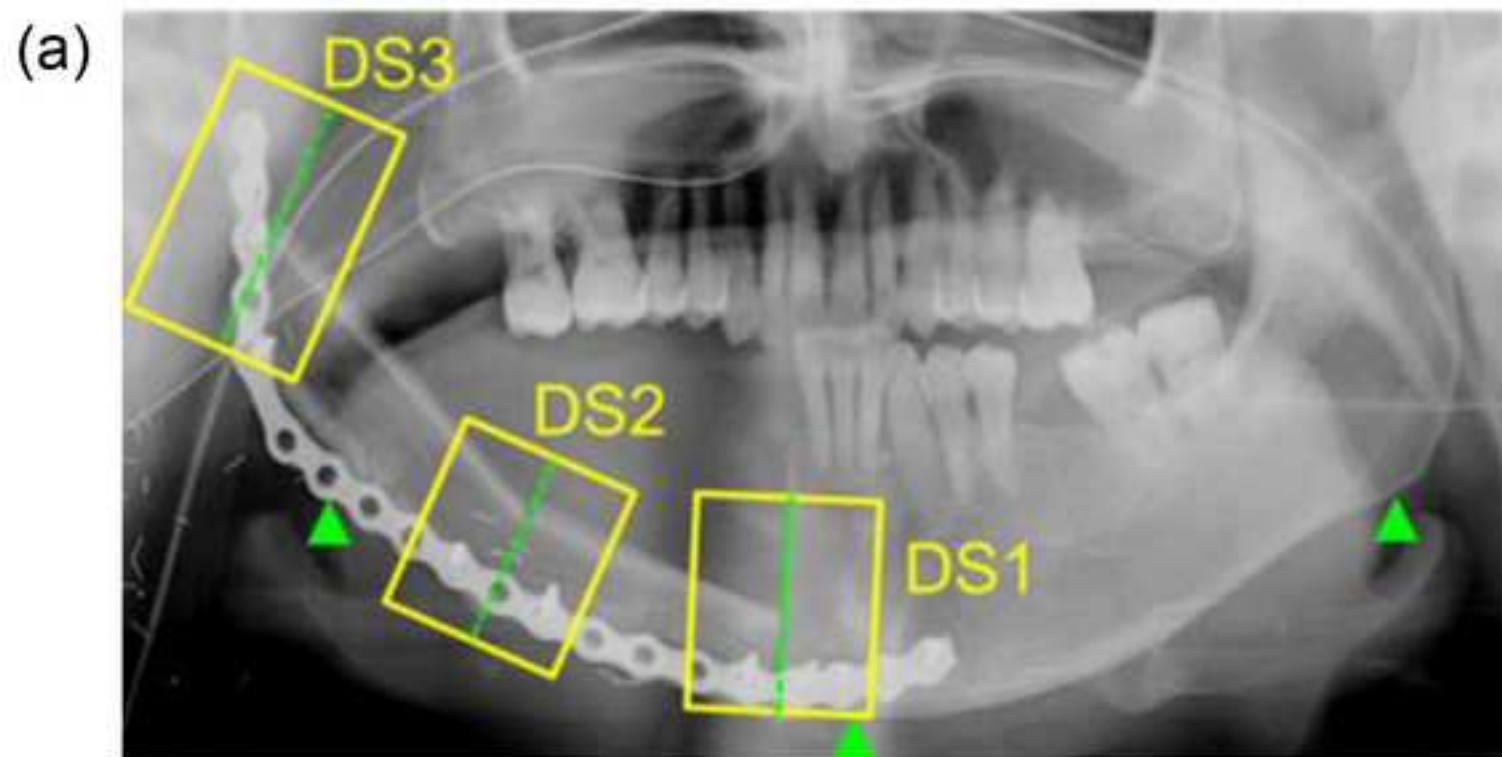


Figure 3  
[Click here to download high resolution image](#)

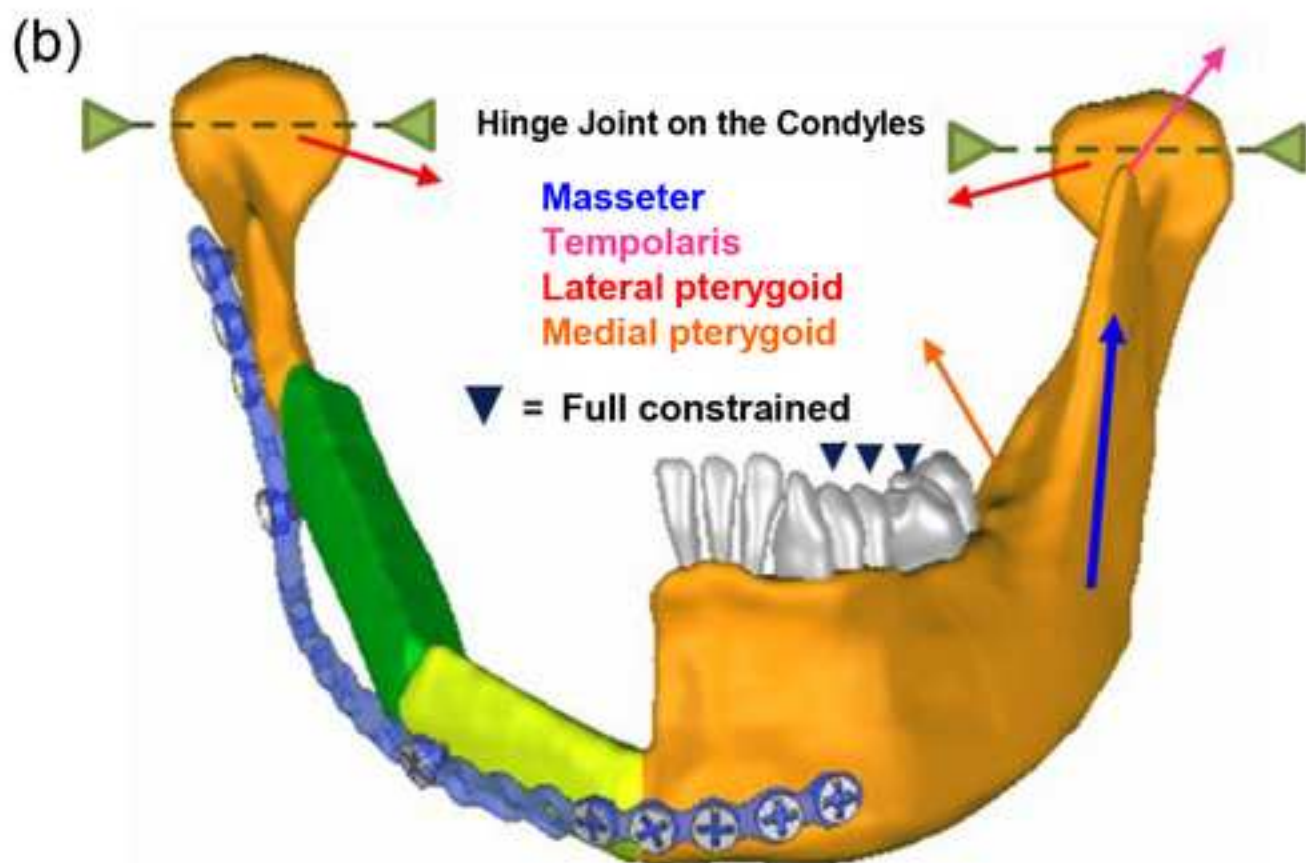
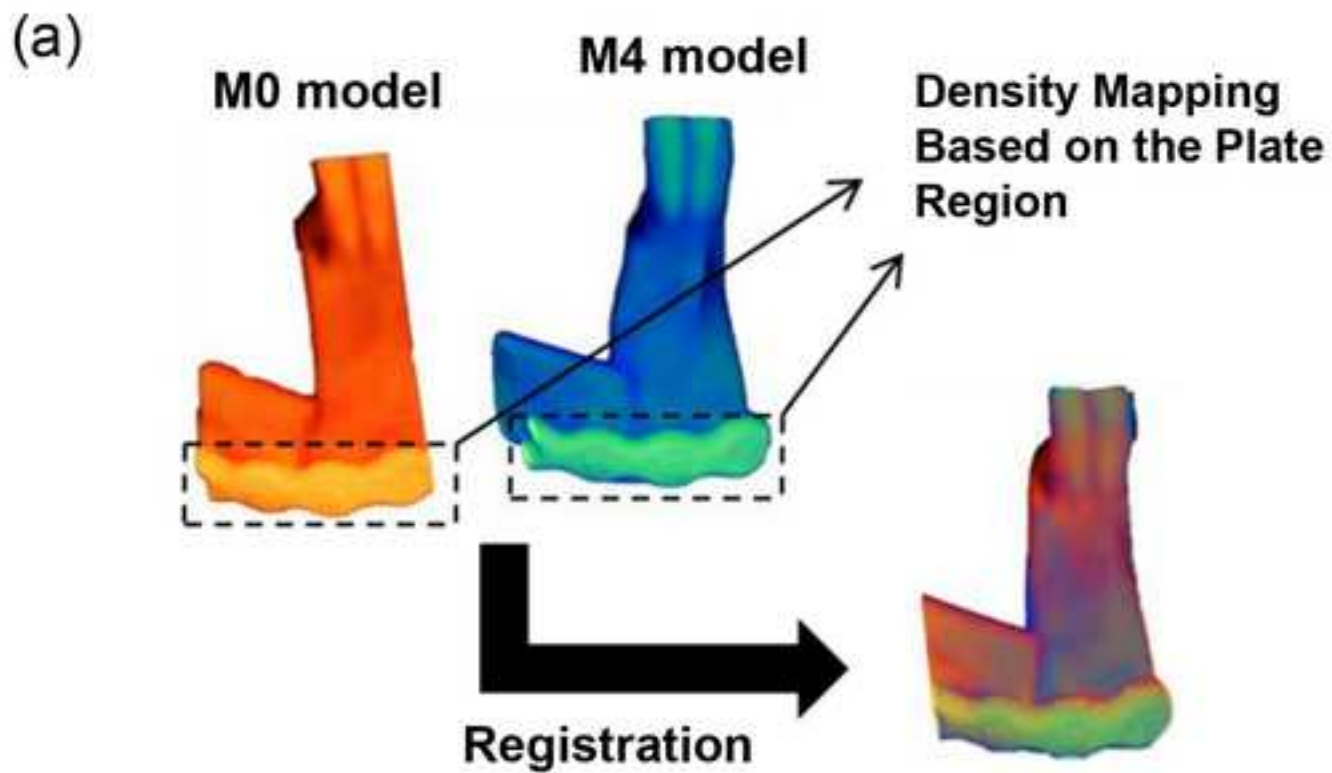


Figure 4

[Click here to download high resolution image](#)

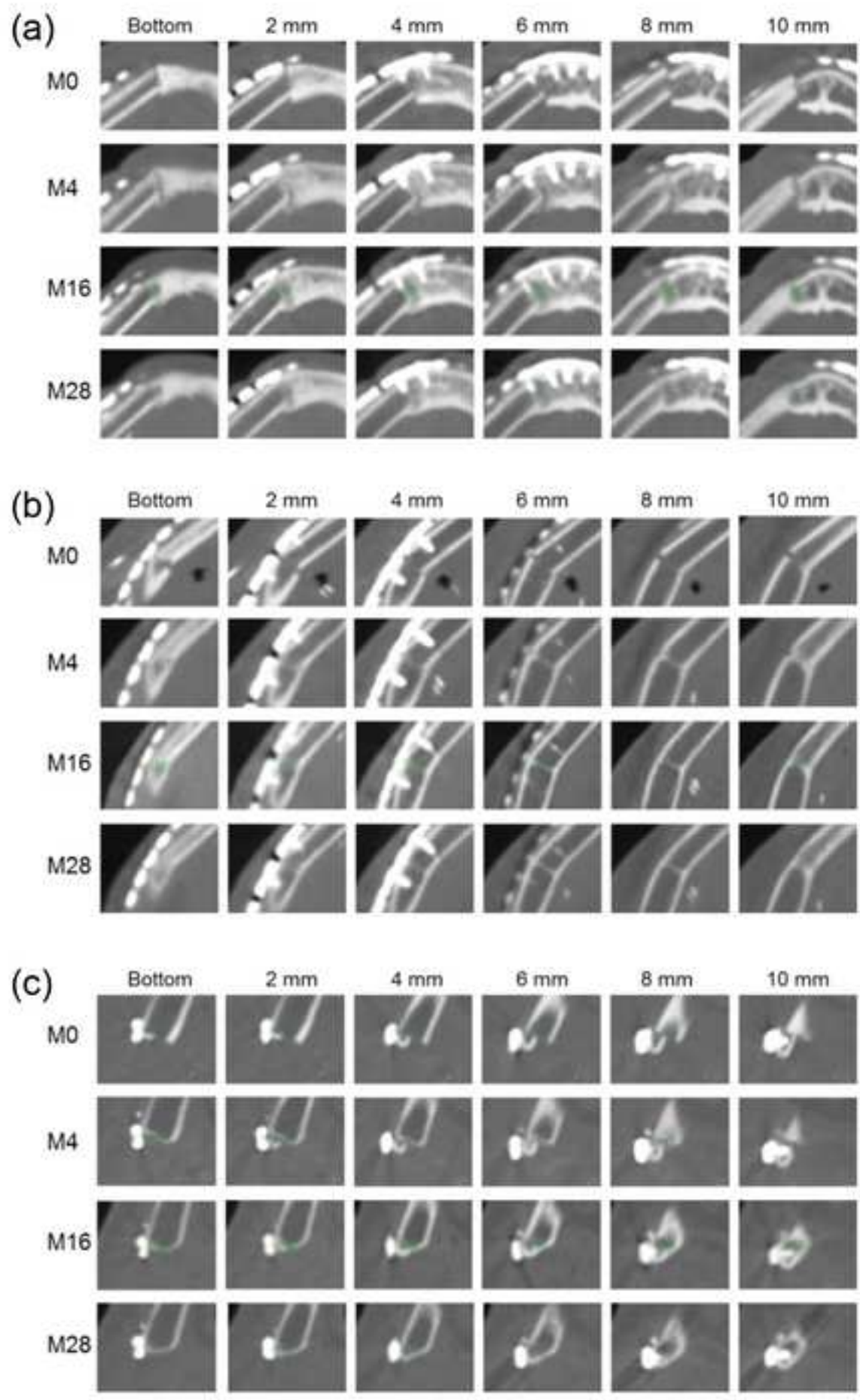


Figure 5  
[Click here to download high resolution image](#)

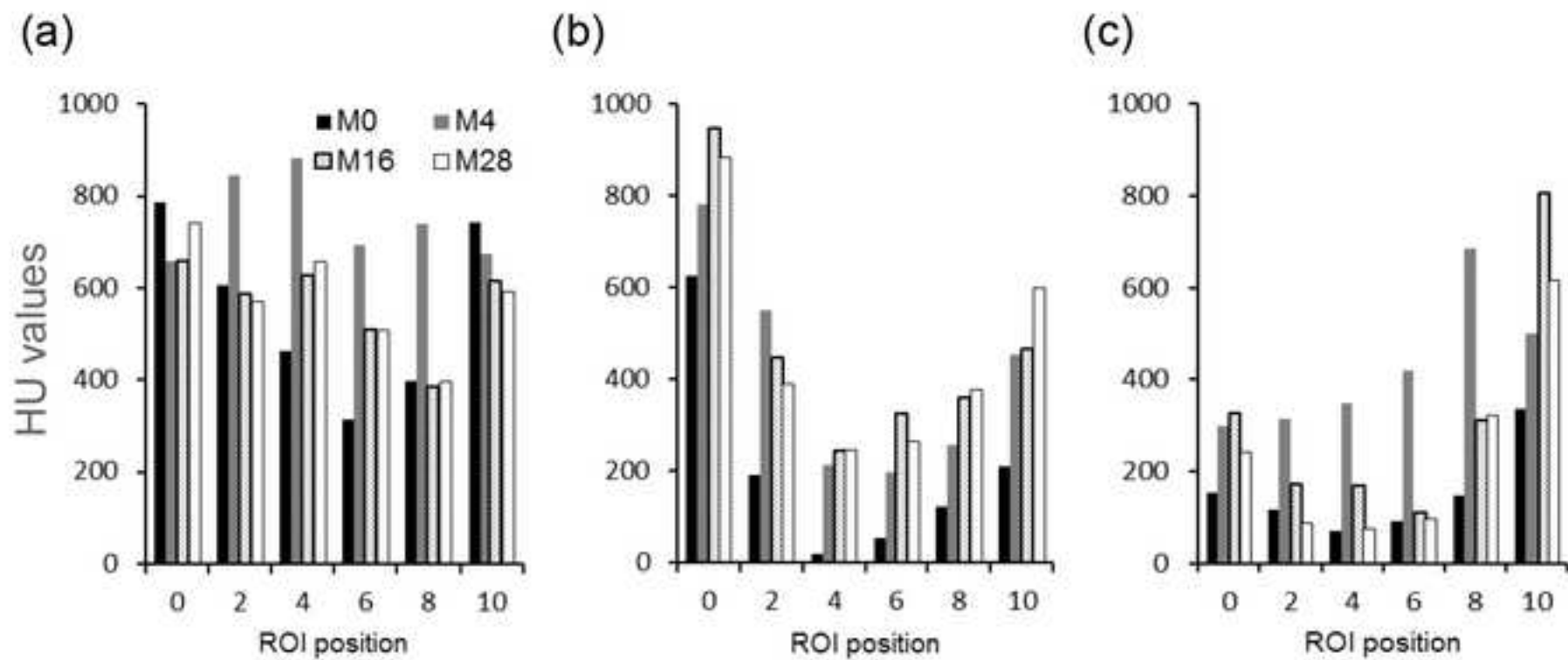


Figure 6  
[Click here to download high resolution image](#)

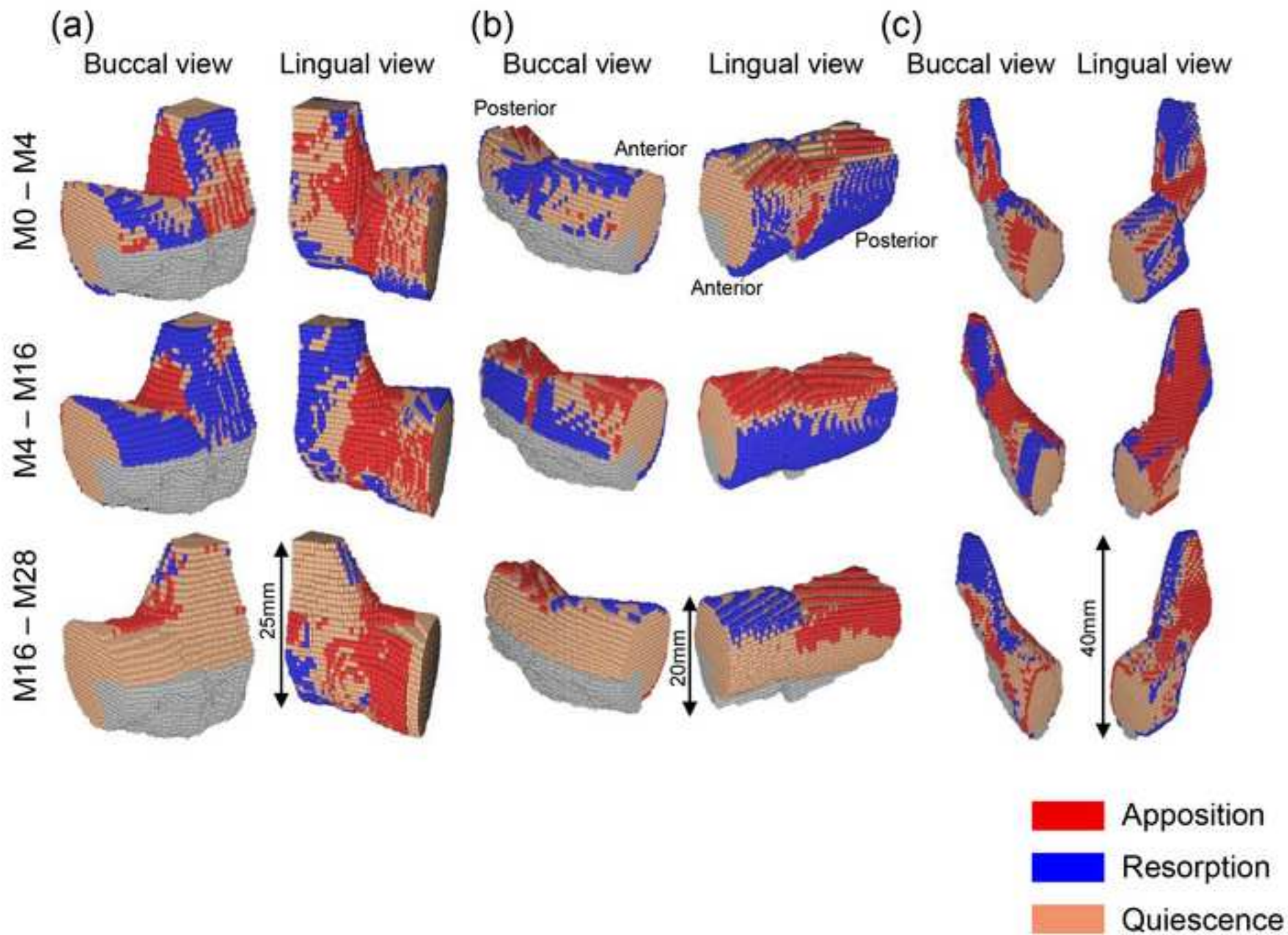


Figure 7  
[Click here to download high resolution image](#)

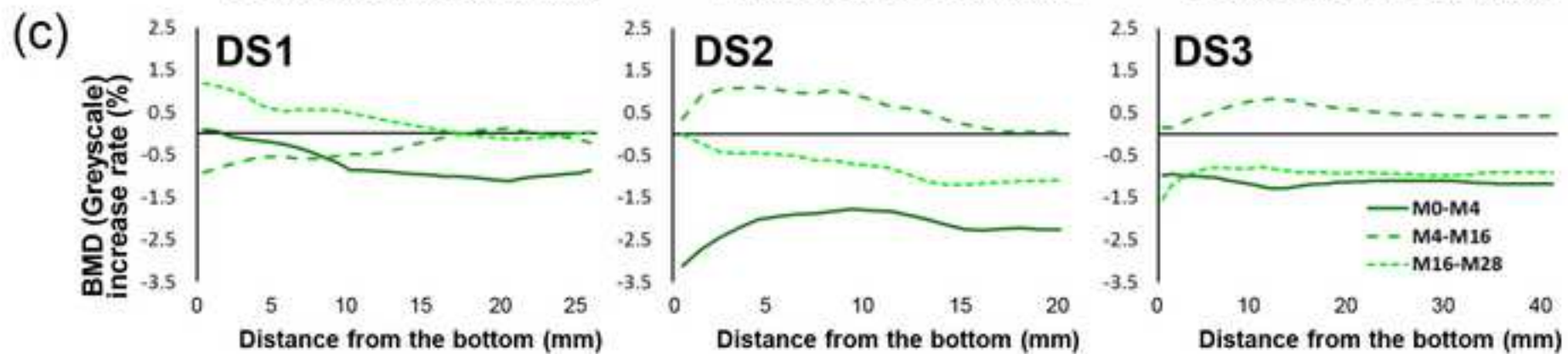
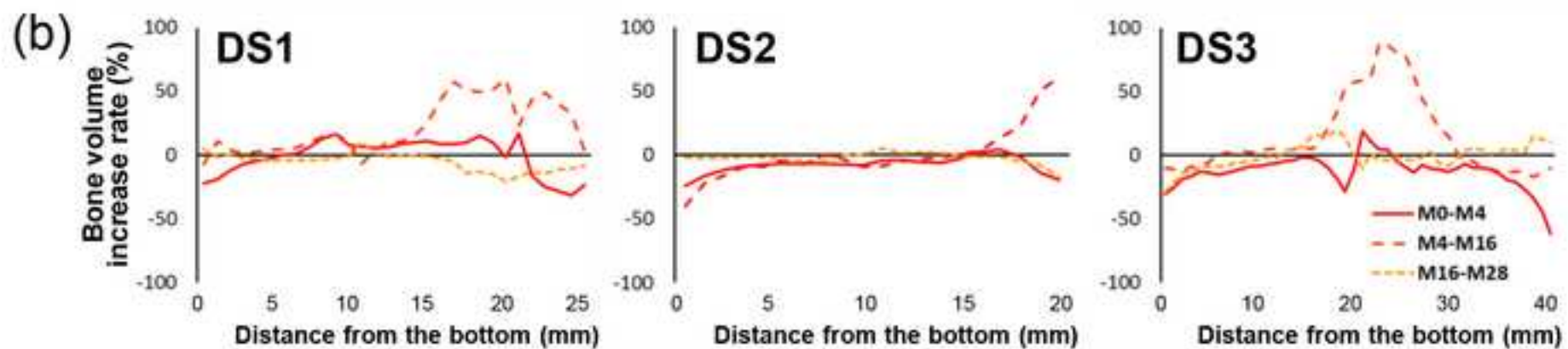
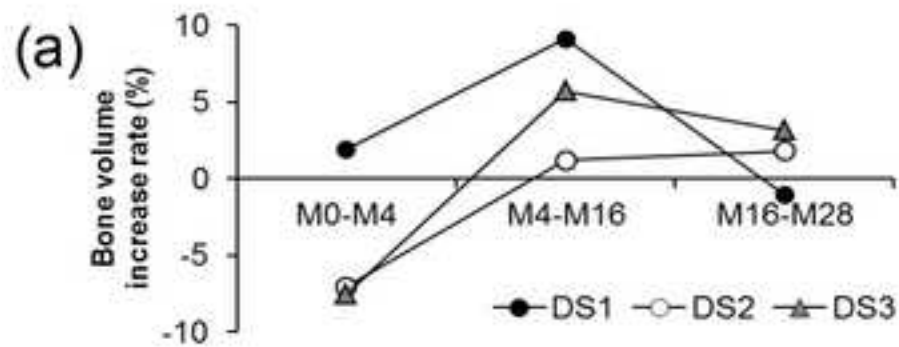


Figure 8  
[Click here to download high resolution image](#)

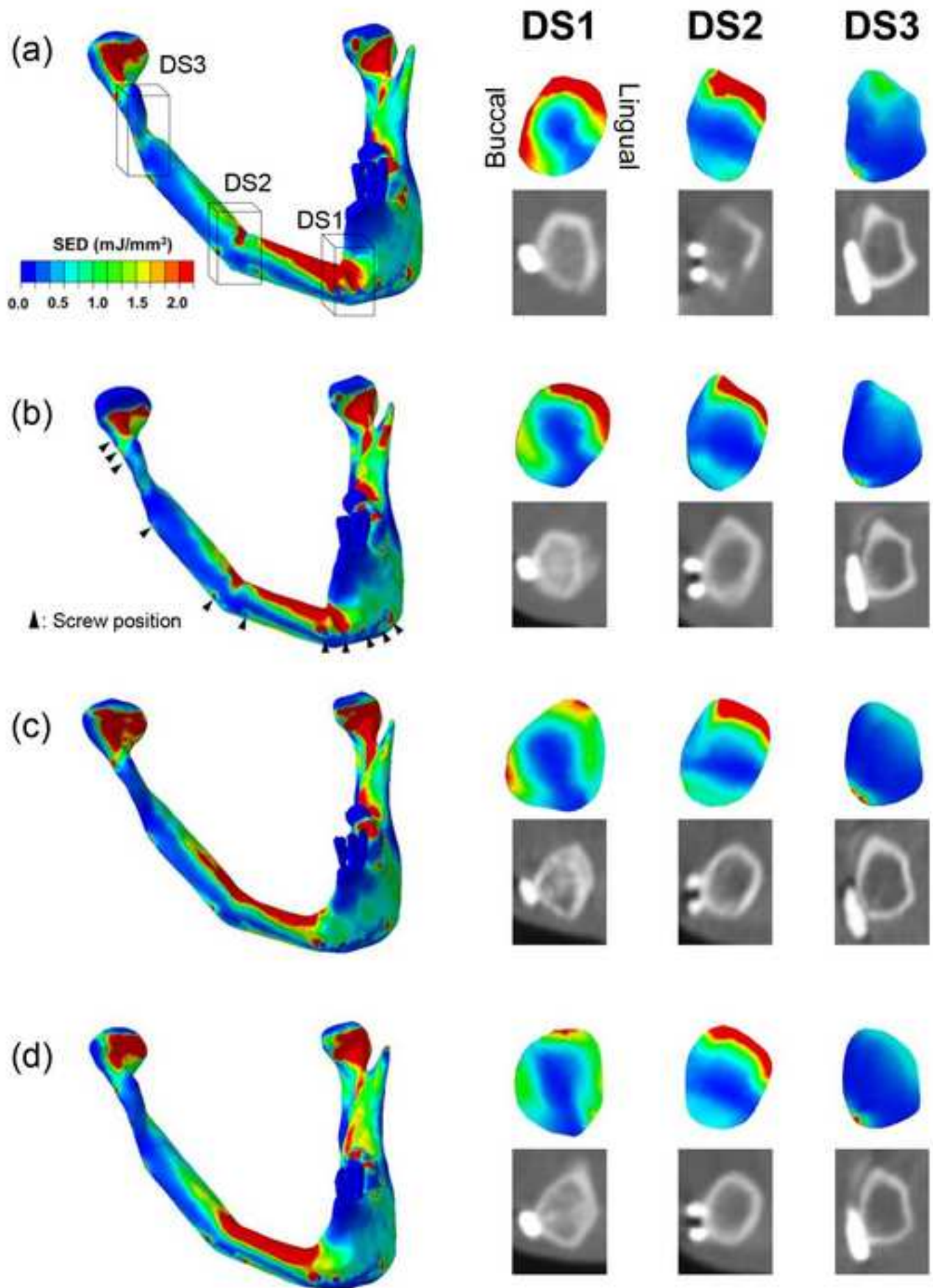


Figure 9  
[Click here to download high resolution image](#)

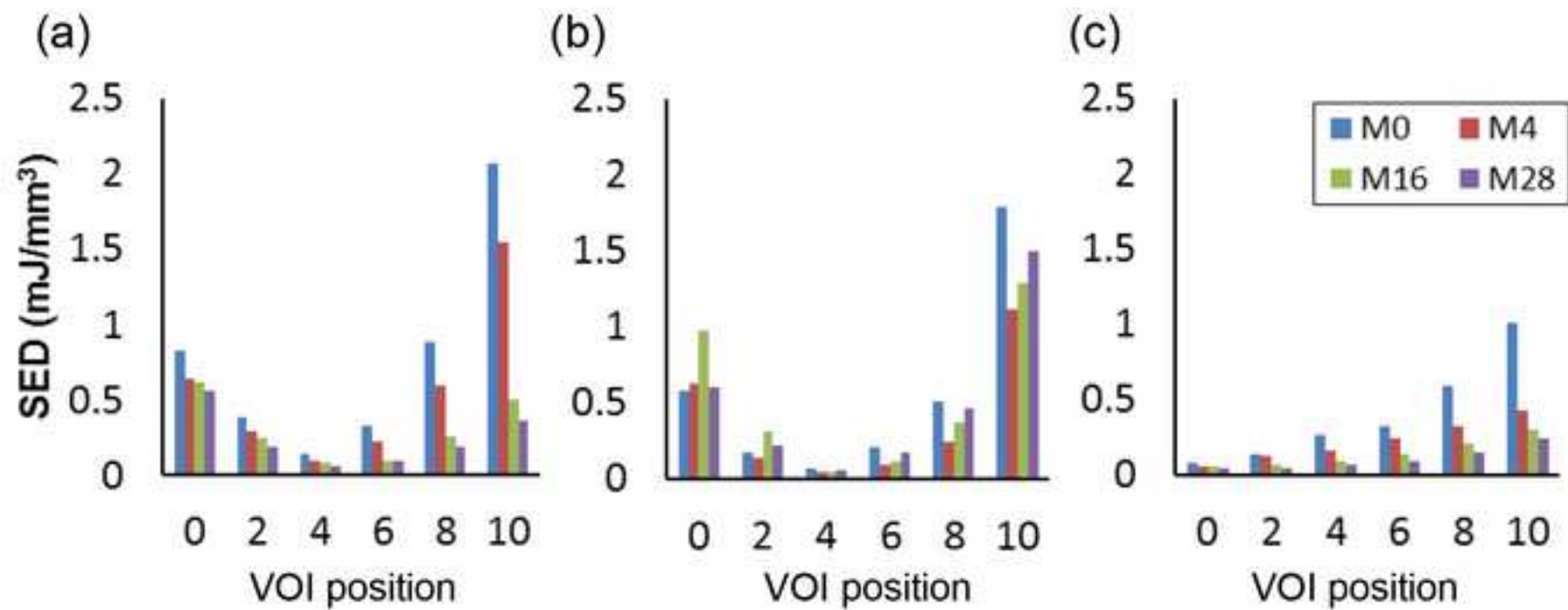




Figure 10  
[Click here to download high resolution image](#)

